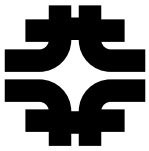

Fermi National Accelerator Laboratory

FERMILAB-FN-642
CMS-TN/96-058

Missing E_T+ Jets Signals for Supersymmetry in the CMS Detector at the LHC

I. Gaines et al.

Fermi National Accelerator Laboratory
P.O. Box 500, Batavia, Illinois 60510

June 1996

Operated by Universities Research Association Inc. under Contract No. DE-AC02-76CHO3000 with the United States Department of Energy

Disclaimer

Fermilab–FN–642
CMS–TN/96–058

Missing E_T+ Jets Signals for Supersymmetry in the CMS Detector at the LHC

I. Gaines*, D. Green*, S. Kunori†, S. Lammel*, J. Marraffino*, J. Womersley*[1], and W. Wu*

* *Fermi National Accelerator Laboratory, Batavia, IL 60510*
† *University of Maryland, College Park, MD 20742*

April 16, 1996

We have studied the potential for observation of supersymmetry through an excess of events with large missing transverse energy accompanied by jets using a parametrized simulation of the CMS detector. We have investigated the use of kinematic selection cuts to select the signal and reject the backgrounds. We find that signal to background ratios greater than unity can be obtained for gluino masses over the whole range 250-1000 GeV. We also find that the QCD multijet background is very sensitive to the calorimeter coverage and resolution. Non-gaussian tails in particular should be avoided.

INTRODUCTION

Supersymmetry at the electroweak scale provides an appealing theoretical framework in which to embed the Standard Model; its successes (such as precision electroweak predictions) are retained, while avoiding any fine tuning of the Higgs mass and ensuring unification of gauge couplings at the GUT scale. Supersymmetric models predict a large spectrum of presently unobserved particles. Many of these will be detectable in the CMS detector at the LHC. In this note we will explore the potential for just one channel: $\tilde{q}, \tilde{g} \rightarrow \tilde{\chi}_i^{\pm,0} + X \rightarrow \tilde{\chi}_1^0 + X$. The lightest supersymmetric particle, $\tilde{\chi}_1^0$, escapes from the detector, giving rise to a signal at large $\not\!\!E_T$. The signal to background can be improved by requiring hard jets from cascade decays in association with the $\not\!\!E_T$.

The motivations for this study were to:

- ensure that the CMS hadron calorimeter will not introduce significant instrumental backgrounds that might impair the ability to observe supersymmetry signals;
- ensure that supersymmetry can be detected down to the relatively low mass scales ($m_{\tilde{g}} \sim 300 - 400\,\mathrm{GeV}$) that can be reached at the Tevatron [1], which is important if there is to be no unexplored "window" between the Tevatron and LHC;
- develop a set of kinematic cuts that maximise the signal to background ratio.

[1] Contact: `womersley@d0sft.fnal.gov`, `http://d0sgi0.fnal.gov/~womersle/womersle.html`

EVENT GENERATOR STUDIES

Before studying the impact of instrumental effects, it is advisable to establish the boundaries and develop a strategy for the later work. From the experimental point of view the most challenging SUSY scenario for the classic missing E_T approach is the one with heavy squarks, so that the observed signal comes almost entirely from gluino pair production. For heavy gluinos the direct decay into LSP has very little branching ratio, thus yields few events with striking $\not\!\!E_T$ signature. The cascade decays of the gluino (for example $\tilde{g} \to qq'\tilde{\chi}^{\pm} \to qq'qq'\tilde{\chi}_1^0$), however, enhance the multijet part of this analysis approach.

Standard Model processes with similar signature will provide an irreducible background. Missing E_T due to neutrinos will be indistinguishable from the one induced by escaping LSPs. Neutrinos are produced in all kinds of SM processes involving on-shell or virtual W and Z bosons. Highly energetic quarks can radiate off a Z that with subsequent decay into neutrinos produces real missing E_T in QCD type multijet events. Although the cross-section of such events is relatively small, the high selectivity of the LHC experiments will make them visible.

At the generator level, we have considered three groups of processes as potential background in the missing E_T plus multijet SUSY search: QCD multijet production includes gluon and light quark production; heavy flavour production includes charm, bottom, and top production; and in the electro-weak group we included Drell-Yan, W, and Z (plus multijet), and diboson (WW, WZ, and ZZ) production.

For this generator level study we used the initial LHC center of mass energy of 10 TeV. ISAJET v7_06 was used with default cross-sections for all generations. Missing E_T is calculated as transverse component of the vector sum of all neutrinos and LSPs in an event. Jets are constructed as clusters of visible particles (i.e. excluding neutrinos and LSPs) with a simple fixed-cone two-step jet finding algorithm. To present the results consistently, a jet with E_T of at least 80 GeV is mandatory for each event.

Figure 1 shows the missing E_T spectrum for an "ideal detector". In $1(a)$ the sum of all SM processes together with gluino pair production for three different gluino masses; in $1(b)$ the contribution from QCD multijet production; in $1(c)$ the contribution from heavy flavour production and individually charm plus beauty and top production; and in $1(d)$ the contribution from electro-weak processes together with the individual contributions. At low missing E_T QCD multijet is the dominant contribution. As missing E_T increases, heavy flavour production takes the leading role, yielding to electro-weak processes as most important contribution at high missing E_T.

A first step towards incorporating instrumental effects is to include the geometrical acceptances for muons and showering particles. Muons are considered lost if their pseudorapidity is $|\eta| > 2.6$ and included in the missing E_T calculation. All other particles are considered lost and source of missing E_T if their pseudorapidity is $|\eta| > 5.0$. In a second step the granularity of the calorimeter is simulated. The impact of these instrumental effects on the missing E_T spectrum is shown in figure 2. It is rather small. However, it causes the QCD multijet to extend as dominant contribution to higher missing E_T. We can expect a similar effect from calorimeter resolution and non-Gaussian tails. For an effective missing E_T based SUSY search it is important to minimize this effect.

PSEUDORAPIDITY COVERAGE

We also used generator-level simulation to revisit the question of the necessary extent of pseudorapidity coverage for the calorimeter, in particular the very forward calorimeter. The $\not\!\!E_T$ distributions for QCD dijet events with at least one jet above 80 GeV were plotted for different $|\eta|$ coverage, starting with $|\eta| < 5.0$ and reducing the limit of $|\eta|$ in steps of 0.1 unit. Down to to $|\eta| < 4.8$ no effects are visible; below that the $\not\!\!E_T$ distribution begins to degrade (see Fig. 3). We conclude that fiducial coverage of at least $|\eta| < 4.8$ is required and thus the actual calorimeter coverage should be greater than this by approximately the width of a hadronic shower.

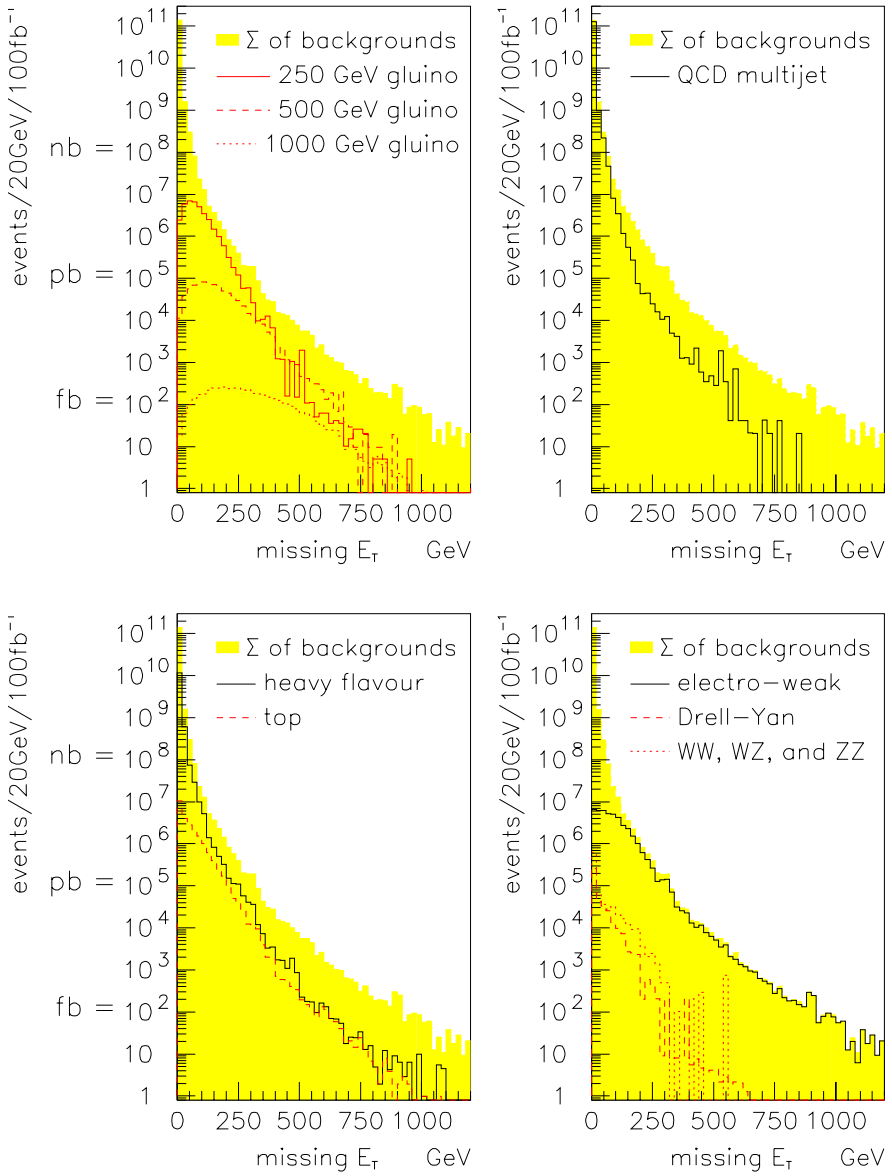

FIG. 1. Distributions of $\not\!\!E_T$ for an "ideal detector". (*a*) the sum of all SM processes together with gluino pair production for three different gluino masses; (*b*) contribution from QCD multijet production; (*c*) contribution from heavy flavour production and individually charm plus beauty and top production; (*d*) contribution from electroweak processes together with the individual contributions.

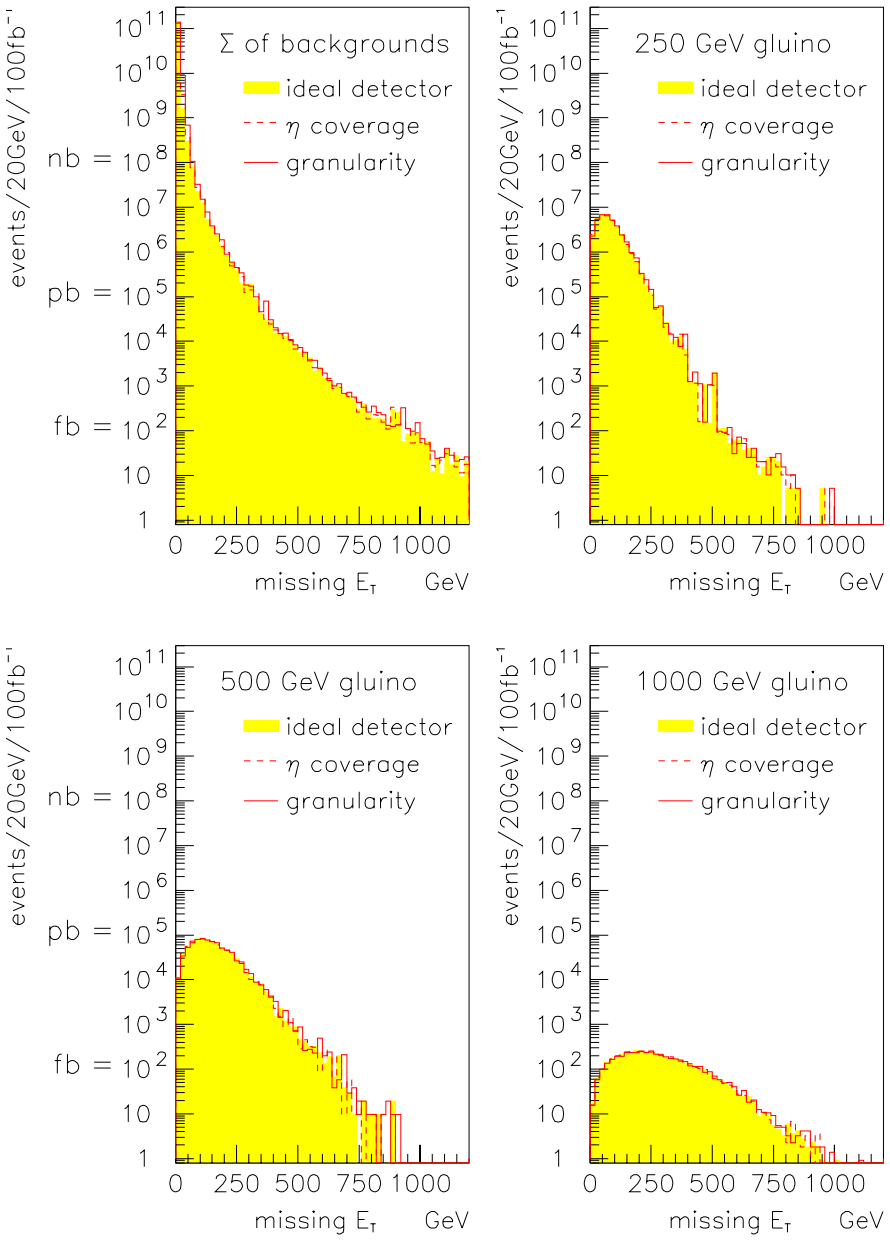

FIG. 2. As Fig. 1 but with coverage limits of $|\eta| \leq 2.6$ for muons and $|\eta| \leq 5.0$ for all other particles, and including calorimeter granularity.

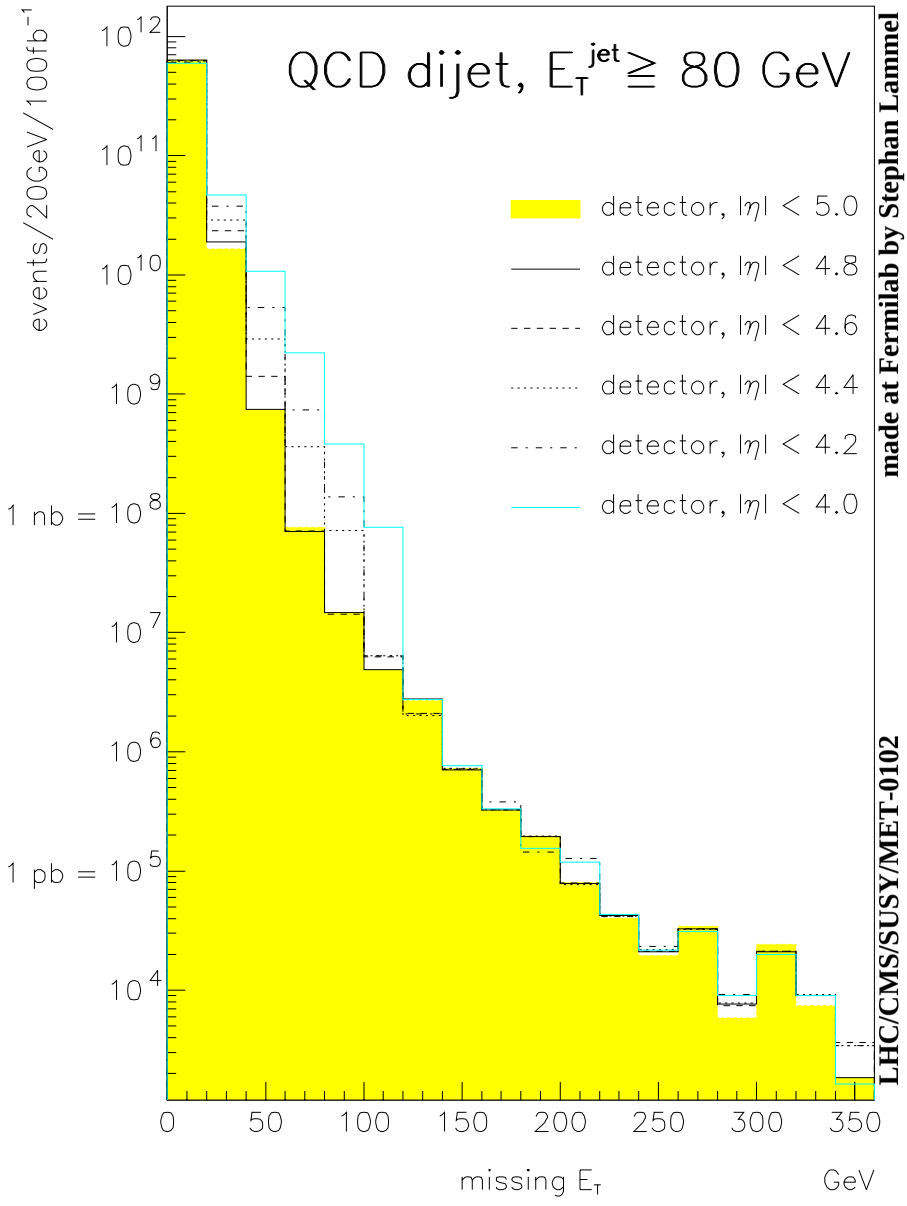

FIG. 3. Missing E_T from QCD multijet events (requiring $E_T^{jet} \geq 80\,\mathrm{GeV}$) for ideal calorimeters of various pseudorapidity coverages.

PARAMETRIZED DETECTOR STUDIES

To study detector effects in more detail, we will use a parametrized simulation of the CMS detector. A parametrized approach is desirable given the large statistics required. The fast simulation used was first developed for the SDC detector [2]. It incorporates:

- stable particles are tracked in the magnetic field (assumed uniform) up to the calorimeter;
- EM calorimetry covers up to $|\eta| = 2.6$, and hadronic up to $|\eta| = 5.0$;
- energy resolution is simulated by Gaussian smearing with sampling and constant terms as below:

	Barrel	Endcap		Very Forward
	$\|\eta\| \leq 1.5$	$1.5 \leq \|\eta\| \leq 2.6$	$2.6 \leq \|\eta\| \leq 3.0$	$3.0 \leq \|\eta\| \leq 5.0$
EM:				
Sampling	0.02	0.02	0.36	0.50
Constant	0.005	0.005	0.03	0.03
Hadronic:				
Sampling	0.65	0.83	0.83	1.00
Constant	0.05	0.05	0.05	0.05

- transverse shower shape is modelled, with an rms width of 7 cm (hadronic) and 0.7 cm (EM);
- shower leakage is modelled, using parametrized test beam data, for calorimeter depths of 8.7λ for $|\eta| \leq 1.5$, 11λ for $1.5 \leq |\eta| \leq 3.0$, and 12λ for $3.0 \leq |\eta| \leq 5.0$;
- cracks in azimuthal coverage are modelled as 2 cm wide regions in the calorimeter where the response is zero at present (this is very much a worst-case assumption);
- energy is stored in cells with transverse segmentation of 0.1×0.1 for all calorimeters.

Jets are then found using a cone algorithm ($R = 0.7$) on the calorimeter tower energies. No minimum bias pileup events were added for these studies.

EVENT SAMPLES

Signal and background events were generated using ISAJET version 7.09. The samples used were:

- Supersymmetry signal events with $(m_{\tilde{g}}, m_{\tilde{q}}) = (250, 750); (500, 1000); (1000, 1500)$ and $(1000, 1000)\,\mathrm{GeV}$. These are referred to as SUSY sets I–IV respectively. For all cases $\tan(\beta) = 4$ and $\mu = -400$; the full set of ISAJET parameters used is listed in Table I. Clearly these choices are only a sample of the full parameter space.
- QCD multijet background events, with gluon, u, d, s, c and b flavored jets. Four ranges of jet transverse momentum were generated, $p_T = (80-300)$, $(300-800)$, $(800-1500)$ and $(1500-3000)$ GeV/c. The QCD background contributes because of $\not\!\!E_T$ from mismeasurement of the jets, and from real neutrinos from b and c quarks. The latter effect is irreducible.
- Top quark production. The same four jet p_T ranges were generated. The $\not\!\!E_T$ here is predominanty due to real neutrinos from W and b decays arising from $t \to Wb$.
- W+jets background. The same four ranges were used for p_T^W. Here the $\not\!\!E_T$ is due to real neutrinos from leptonic W decays.

	SUSY I	SUSY II	SUSY III	SUSY IV
$m_{\tilde{g}}$	250	500	1000	1000 GeV
$m_{\tilde{q}}$	750	1000	1500	1000 GeV
$m_{\tilde{\ell}_L}$	454.3	905.3	1233.7	1233.7 GeV
$m_{\tilde{\ell}_R}$	450.5	898.2	1213.1	1213.1 GeV
$m_{\tilde{\nu}}$	448.0	902.1	1231.4	1231.4 GeV
$m_{\tilde{t}_L}$	500	1000	1500	1000 GeV
$m_{\tilde{t}_R}$	500	1000	1500	1000 GeV
A_t	-100	-100	-100	-100
$m_{\tilde{b}_R}$	500	1000	1500	1000 GeV
A_b	500	1000	1500	1500
$\tan(\beta)$	4.0	4.0	4.0	4.0
μ	-400	-400	-400	-400
m_{hA}	500	500	500	500 GeV

TABLE I. ISAJET parameters used for the supersymmetry signal samples I–IV.

- Z+jets background. The same four ranges were used for p_T^Z. This background contributes because of large $\not\!\!E_T$ from $Z \to \nu\nu$ decays.

We use the ISAJET production cross sections for all of these processes for $\sqrt{s} = 14\,\text{TeV}$ as listed in Table II.

EVENT SELECTION

Events were kept if they passed the following cuts:

- The azimuthal angle between the $\not\!\!E_T$ and the leading jet must be between $160^\circ \leq \Delta\phi \leq 20^\circ$. This reduces the background from events where the $\not\!\!E_T$ is due to mismeasurement of the jet energy and thus reduces sensitivity to calorimeter performance.
- Require at least three jets within $|\eta| \leq 2.5$, with transverse energies satisfying the following cuts (separately optimized for each signal mass range):

Parameter Set	E_{T1}^{min}	E_{T2}^{min}	E_{T3}^{min}
SUSY I	100	80	60 GeV
SUSY II	150	120	90 GeV
SUSY III	240	200	160 GeV
SUSY IV	240	200	160 GeV

These define the minimal set of cuts.

Figures 4–8 show the distributions of $\Delta\phi$ and number of jets passing these cuts. It can be seen that the supersymmetry signal events tend to have a less strongly peaked $\Delta\phi$ distribution and a wider distribution of the number of jets than the backgrounds.

The contribution of each of the individual backgrounds to the total is shown in Figs. 9–11. As expected, the QCD background dominates at low $\not\!\!E_T$ while the W and Z processes dominate at high $\not\!\!E_T$.

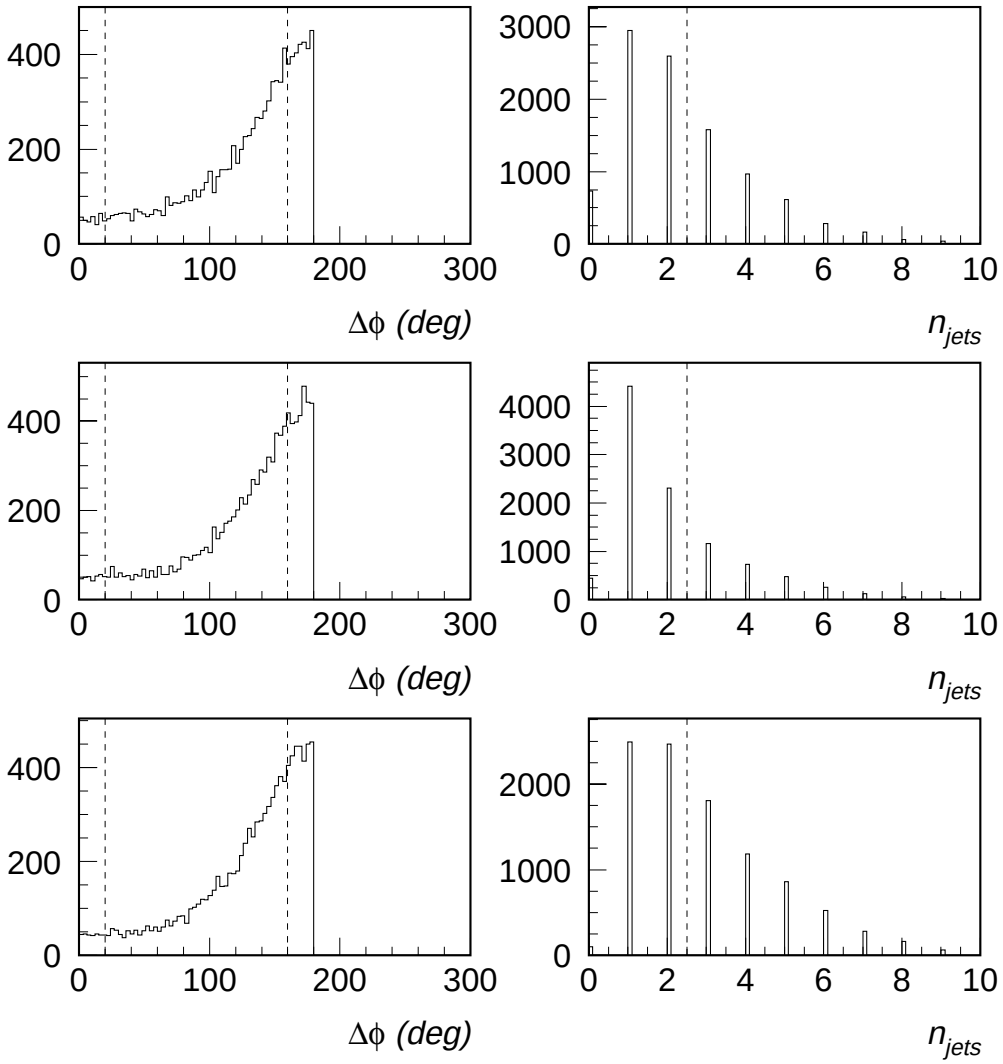

FIG. 4. Distributions of $\Delta\phi$ between $\not\!\!E_T$ and the leading jet (left side) and of the number of jets passing E_T cuts (right side), for SUSY I (upper row), SUSY II (middle row), and SUSY III (lower row), for supersymmetry signal events. Vertical lines indicate the cuts applied.

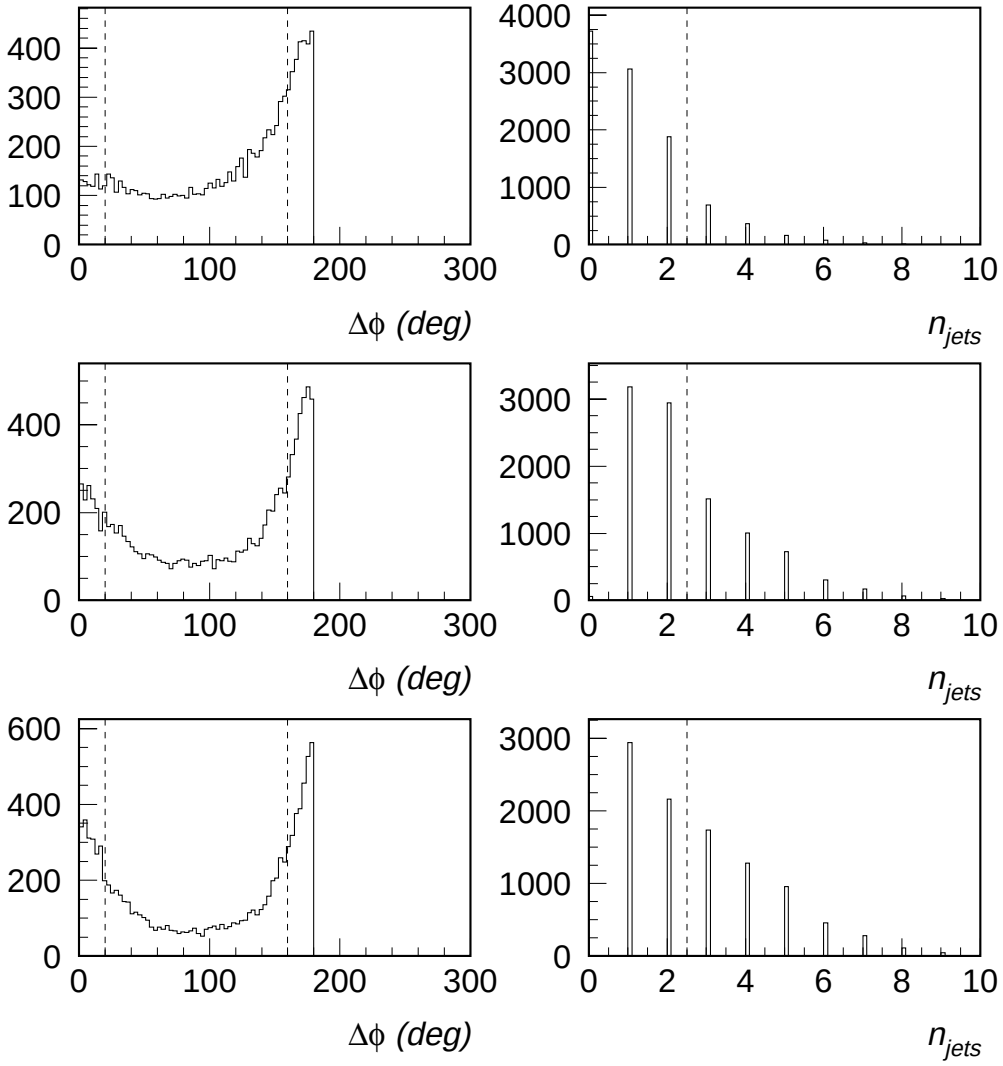

FIG. 5. Distributions for QCD background events of $\Delta\phi$ between $\not\!\!E_T$ and the leading jet (left side), and of the number of jets passing E_T cuts (right side), for $p_T = (80 - 300)\,\mathrm{GeV/c}$ (upper row), $p_T = (300 - 800)\,\mathrm{GeV/c}$ (middle row), and $p_T = (800 - 1500)\,\mathrm{GeV/c}$ (lower row). The jet cuts were appropriate for $m_{\tilde{g}} = 250\,\mathrm{GeV}$ (upper row), SUSY II (middle row), and SUSY III (lower row). Vertical lines indicate the cuts applied.

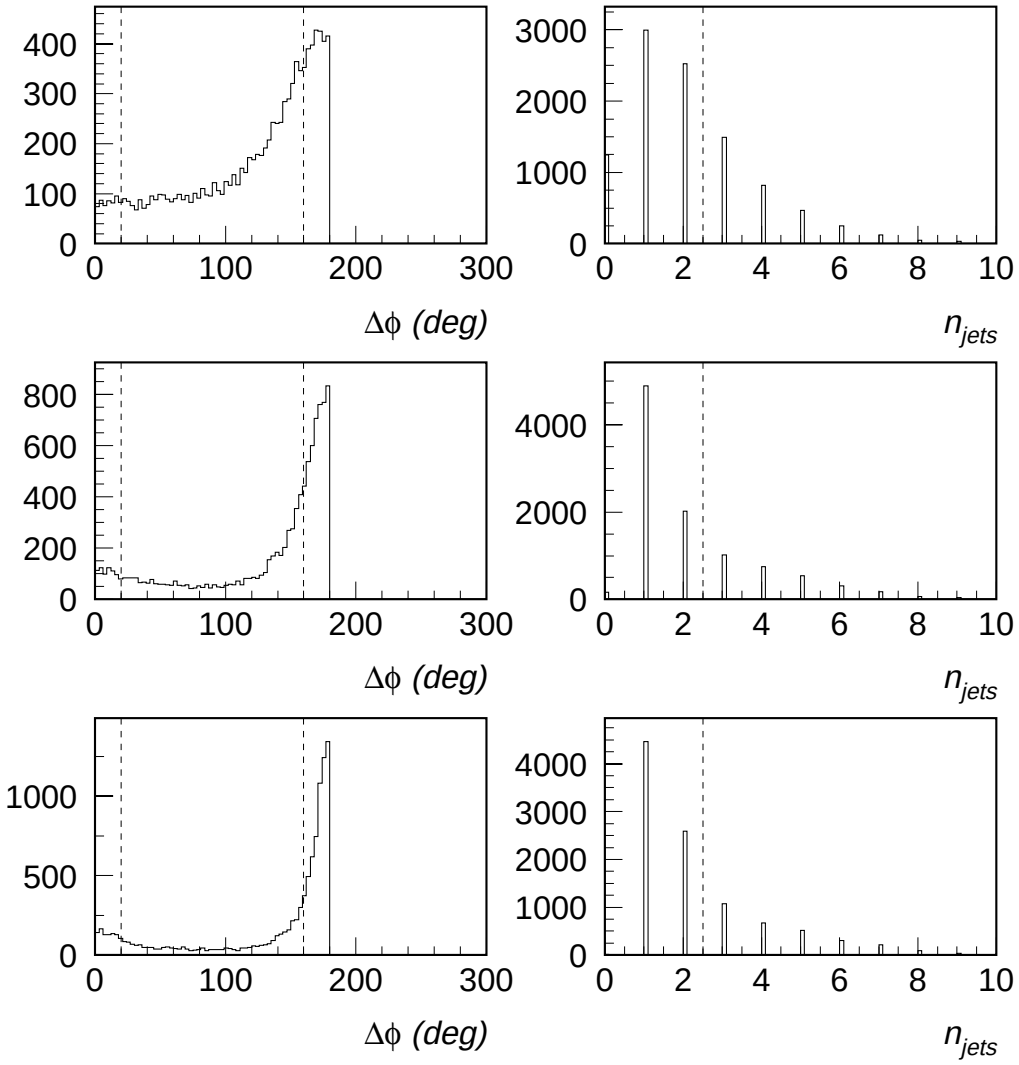

FIG. 6. Distributions for top background events of $\Delta\phi$ between $\not\!\!E_T$ and the leading jet (left side), and of the number of jets passing E_T cuts (right side), for $p_T = (80 - 300)\,\mathrm{GeV/c}$ (upper row), $p_T = (300 - 800)\,\mathrm{GeV/c}$ (middle row), and $p_T = (800 - 1500)\,\mathrm{GeV/c}$ (lower row). The jet cuts were appropriate for $m_{\tilde{g}} = 250\,\mathrm{GeV}$ (upper row), SUSY II (middle row), and SUSY III (lower row). Vertical lines indicate the cuts applied.

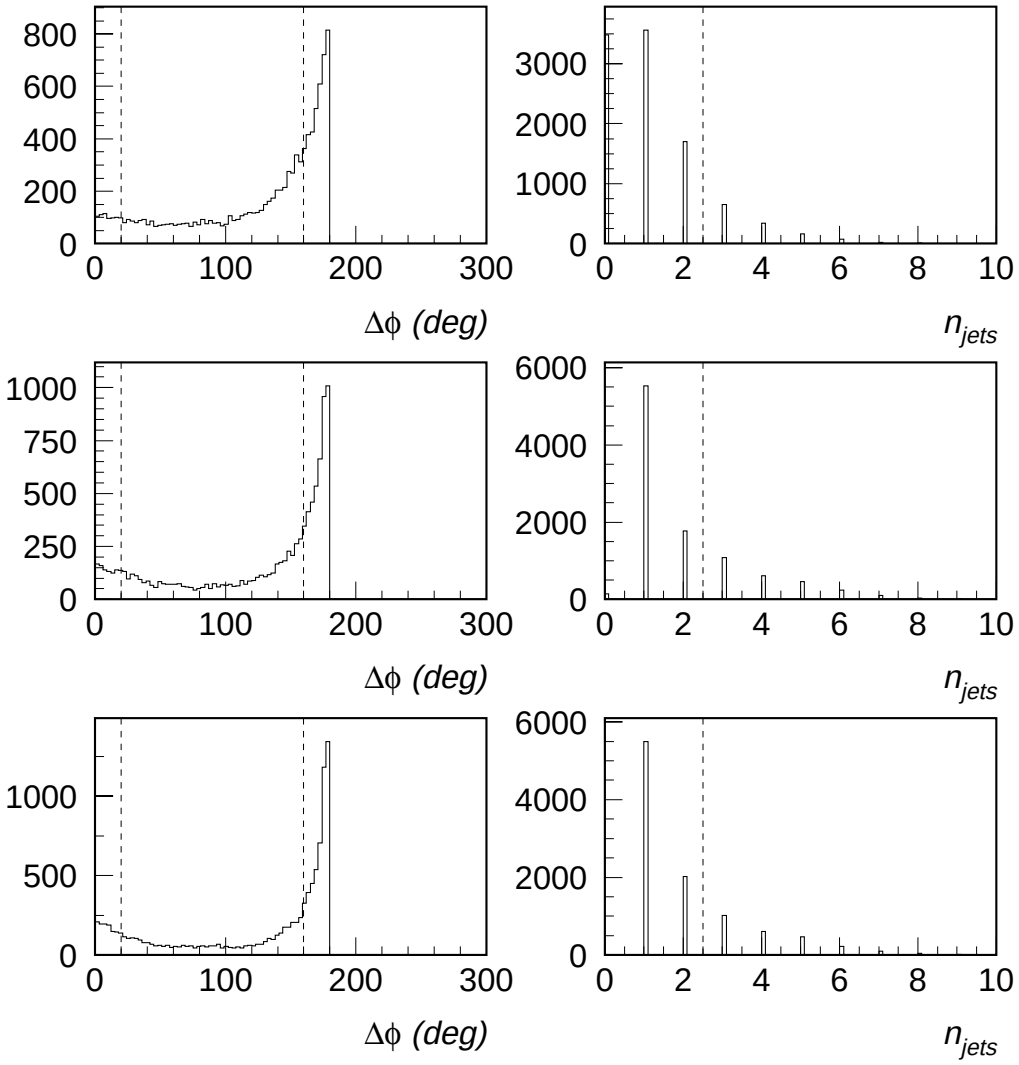

FIG. 7. Distributions for Z+jets background events of $\Delta\phi$ between $\not\!\!E_T$ and the leading jet (left side), and of the number of jets passing E_T cuts (right side), for $p_T = (80 - 300)\,\mathrm{GeV/c}$ (upper row), $p_T = (300 - 800)\,\mathrm{GeV/c}$ (middle row), and $p_T = (800 - 1500)\,\mathrm{GeV/c}$ (lower row). The jet cuts were appropriate for $m_{\tilde{g}} = 250\,\mathrm{GeV}$ (upper row), SUSY II (middle row), and SUSY III (lower row). Vertical lines indicate the cuts applied.

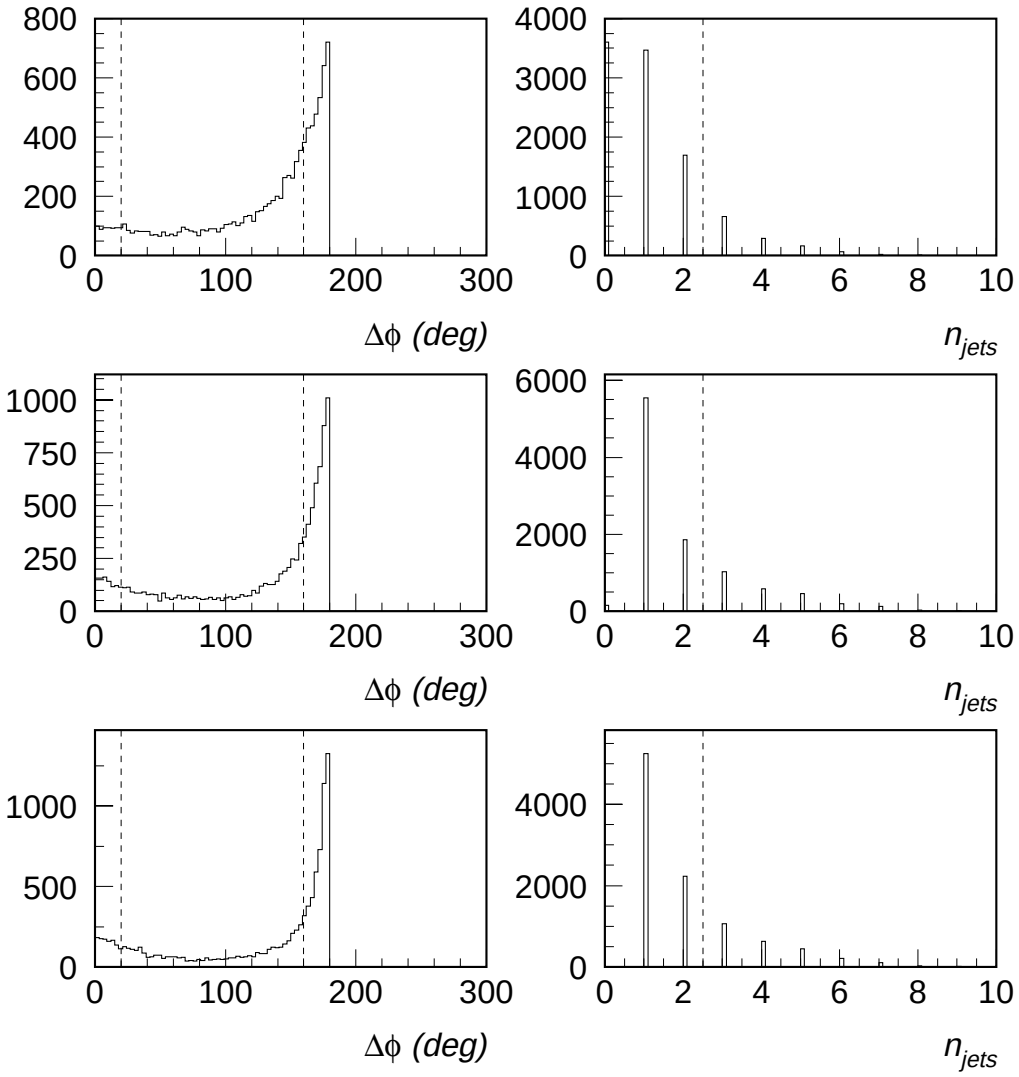

FIG. 8. Distributions for W+jets background events of $\Delta\phi$ between $\not\!\!E_T$ and the leading jet (left side), and of the number of jets passing E_T cuts (right side), for $p_T = (80 - 300)\,\mathrm{GeV/c}$ (upper row), $p_T = (300 - 800)\,\mathrm{GeV/c}$ (middle row), and $p_T = (800 - 1500)\,\mathrm{GeV/c}$ (lower row). The jet cuts were appropriate for SUSY I (upper row), SUSY II (middle row), and SUSY III (lower row). Vertical lines indicate the cuts applied.

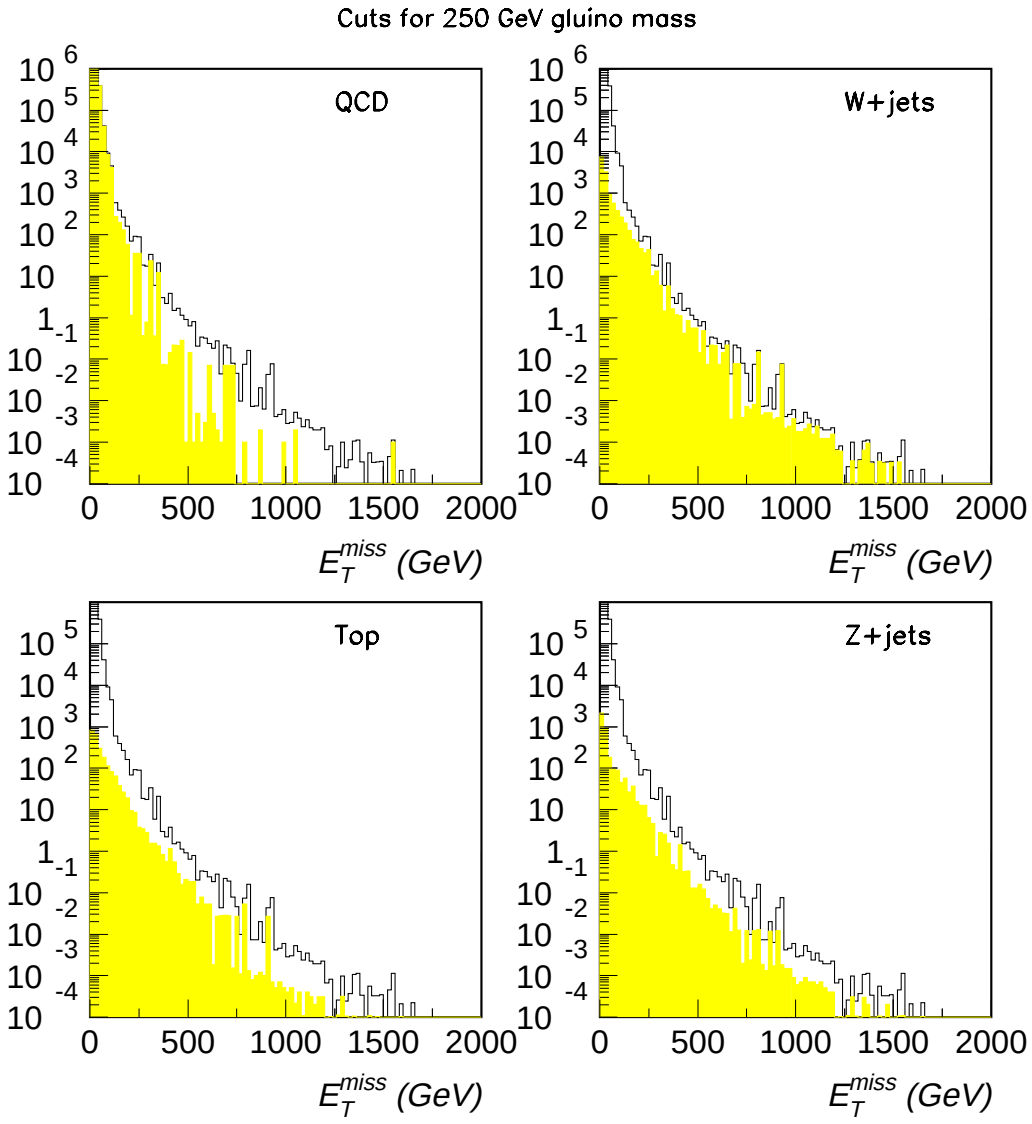

FIG. 9. Contributions of QCD, W+jets, Z+jets and $t\bar{t}$ backgrounds (shaded histograms) to the total background (outline), as a function of $\not\!\!E_T$. Jet cuts appropriate for SUSY I.

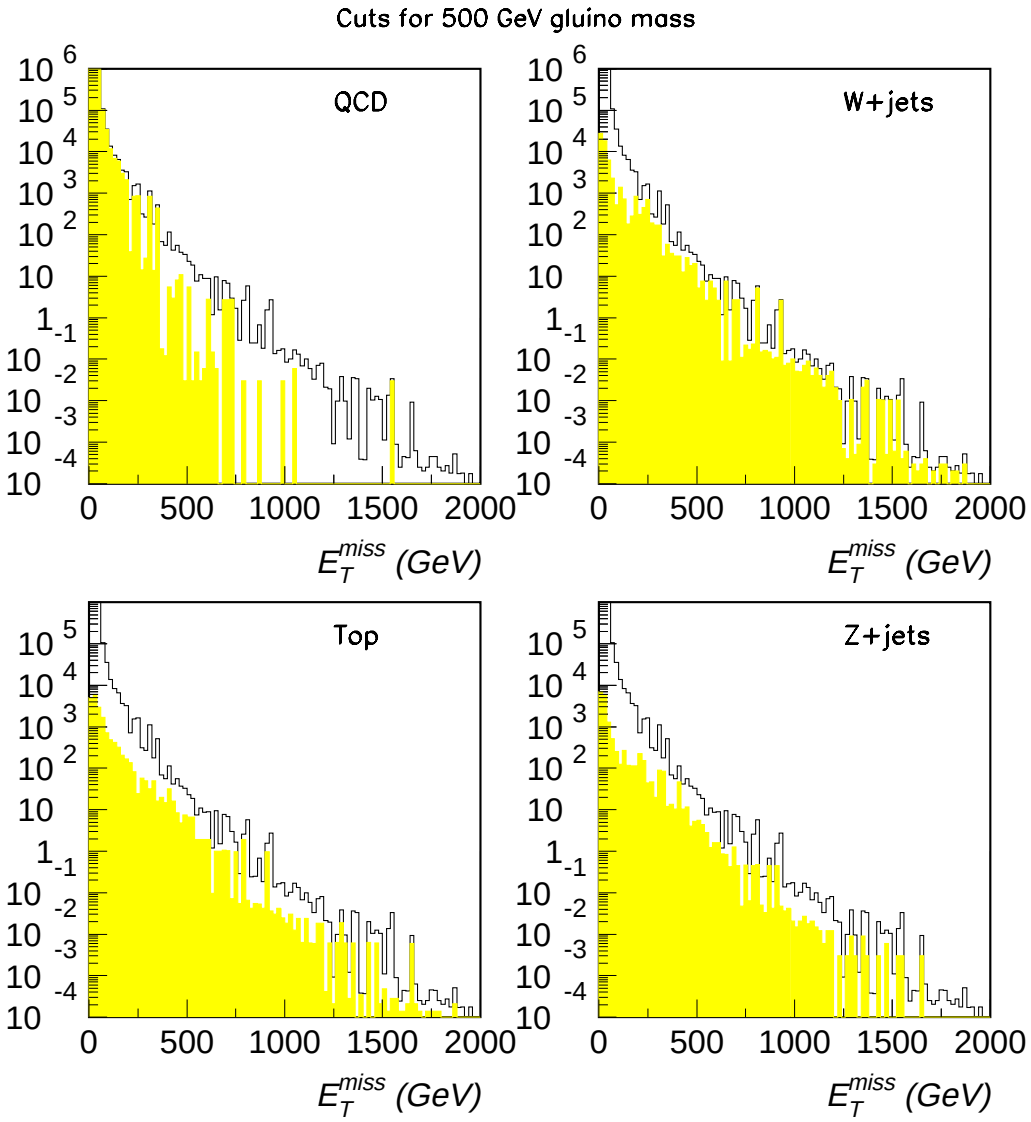

FIG. 10. Contributions of QCD, W+jets, Z+jets and $t\bar{t}$ backgrounds (shaded histograms) to the total background (outline), as a function of $\not\!\!E_T$. As the previous figure, except using jet cuts appropriate for SUSY II.

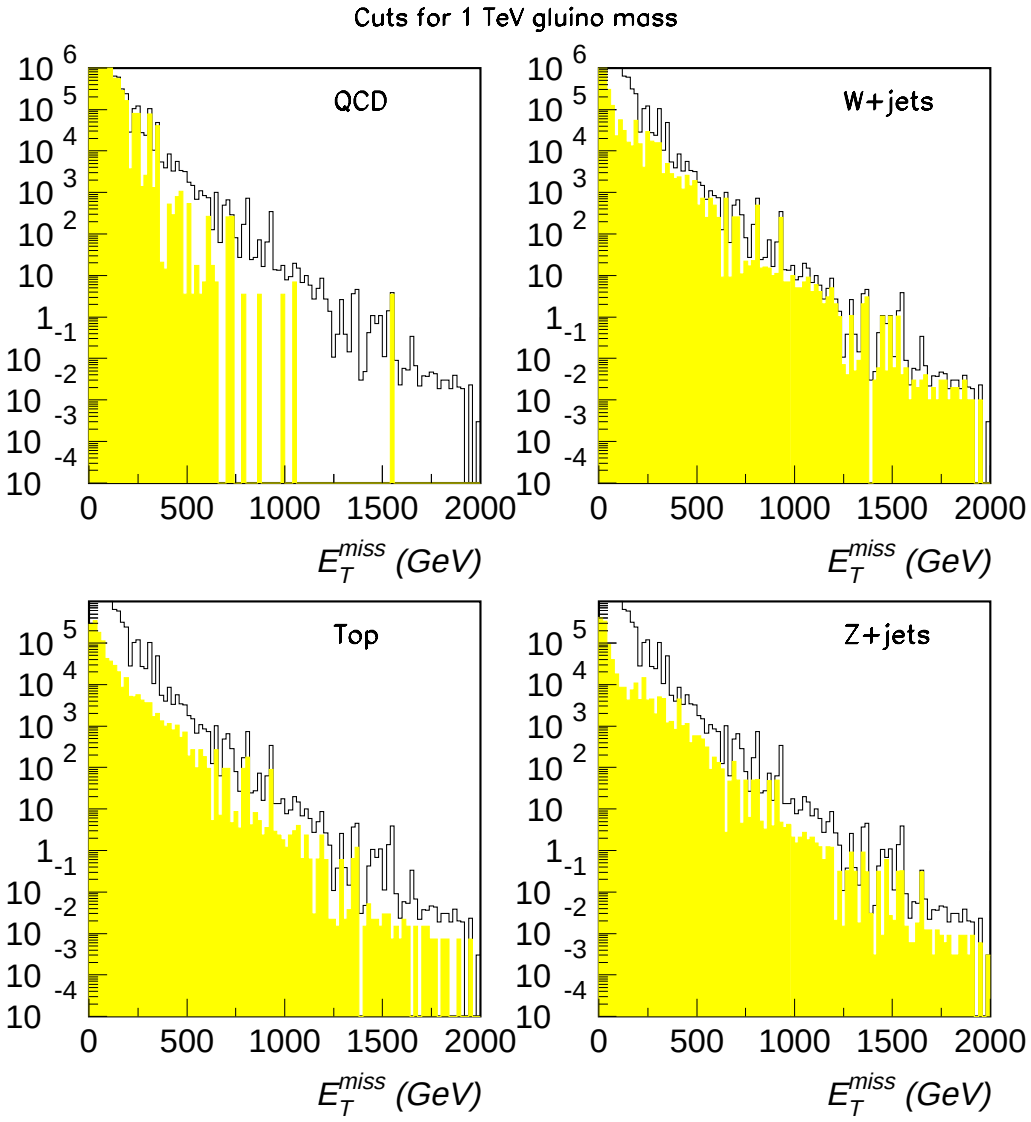

FIG. 11. Contributions of QCD, W+jets, Z+jets and $t\bar{t}$ backgrounds (shaded histograms) to the total background (outline), as a function of $\not{E}_T$. As the previous figure, except using jet cuts appropriate for $m_{\tilde{g}} = 1$ TeV (SUSY III and IV).

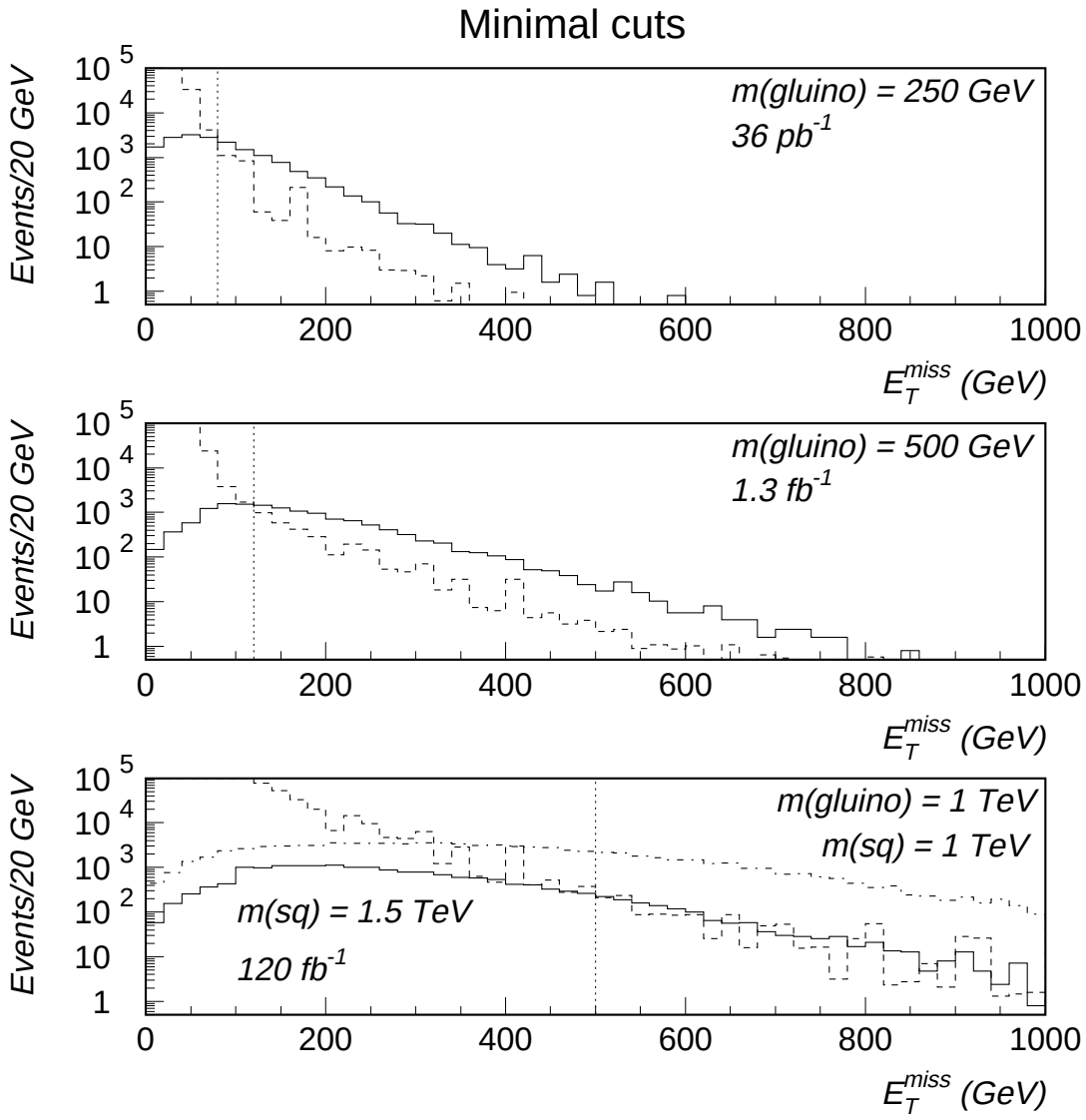

FIG. 12. Distributions of $\not\!\!E_T$ for supersymmetry signal events (solid) and the sum of all backgrounds (dashed), for SUSY I (upper row), SUSY II (middle row), and SUSY III and IV (lower row). Minimal cuts were used. The signal statistics correspond to integrated luminosities of 36 pb^{-1}, 1.3 fb^{-1} and 120 fb^{-1} respectively; the background is normalized to the signal. Vertical lines indicate the signal regions listed in the text.

p_T range (GeV/c)	5–3000			
SUSY I, $m_{\tilde{g}} = 250\,\text{GeV}$	1.1×10^{-6}			
SUSY II, $m_{\tilde{g}} = 500\,\text{GeV}$	3.1×10^{-8}			
SUSY III, $m_{\tilde{g}} = 1\,\text{TeV}$	3.3×10^{-10}			
SUSY IV, $m_{\tilde{g}} = m_{\tilde{q}} = 1\,\text{TeV}$	2.6×10^{-9}			
p_T range (GeV/c)	80–300	300–800	800–1500	1500–3000
QCD	4.2×10^{-3}	1.3×10^{-5}	8.7×10^{-8}	1.2×10^{-9}
$t\bar{t}$	4.8×10^{-7}	2.9×10^{-8}	1.9×10^{-10}	2.5×10^{-12}
W+jets	4.2×10^{-6}	4.0×10^{-8}	3.3×10^{-10}	5.7×10^{-12}
Z+jets	1.1×10^{-6}	1.5×10^{-8}	1.0×10^{-10}	1.7×10^{-12}

TABLE II. Production cross sections (mb) for the supersymmetry signal and background samples, from ISAJET.

The distribution of $\not\!\!E_T$ for signal and the sum of all backgrounds after applying these selection cuts is shown in Fig. 12. The signal can be clearly seen above the backgrounds with:

- $S/B \sim 20$ for $\not\!\!E_T \gtrsim 80\,\text{GeV}$ for SUSY I, with ~ 2000 events per 20 GeV bin for a luminosity of only $36\,\text{pb}^{-1}$;
- $S/B \sim 10$ for $\not\!\!E_T \gtrsim 120\,\text{GeV}$ for SUSY II, with ~ 1000 events per 20 GeV bin for a luminosity of $1.3\,\text{fb}^{-1}$;
- $S/B \sim 2$ for $\not\!\!E_T \gtrsim 500\,\text{GeV}$ for SUSY III, with ~ 200 events per 20 GeV bin for a luminosity of $120\,\text{fb}^{-1}$;
- $S/B \sim 20$ for $\not\!\!E_T \gtrsim 400\,\text{GeV}$ for SUSY IV, with ~ 2000 events per 20 GeV bin for a luminosity of $120\,\text{fb}^{-1}$.

Note that handles exist for understanding the dominant backgrounds at high $\not\!\!E_T$. The Z+jets background can be well-measured in the $\ell\ell$ mode and the $\not\!\!E_T$ distribution simulated from $\ell\ell$ events by discarding the lepton tracks. The W+jets cross section at high p_T^W will be measurable, as will be the $t\bar{t}$ cross section. The QCD background, which is the hardest to calculate since it depends so much on detector performance, is not the dominant background above the quoted $\not\!\!E_T$ cuts.

Additional cuts were investigated with the aim of reducing the W, Z and $t\bar{t}$ backgrounds by rejecting leptonic W decays.

- There must be no electron within $|\eta| \leq 2.5$, $E_T > 10\,\text{GeV}$ and $E_T^{iso} \leq 20\,\text{GeV}$ (within an isolation cone of $R = 0.1$).
- There must be no muon within $|\eta| \leq 2.5$ and $E_T > 10\,\text{GeV}$.

Figure 13 shows the effect of these cuts. As can be seen, the signal to background ratio is actually a little worse than for the minimal cuts. This is because the supersymmetry signal events have a significant number of isolated leptons themselves, arising from cascade decays involving gauginos.

Another possibility investigated was to cut on the transverse mass of the leading electron or muon + $\not\!\!E_T$. This is intended to reject real W's which are expected to have a transverse mass between about 50 and 100 GeV. Figure 14 shows the distributions of transverse mass for the various event samples. A small peak around 80 GeV can be seen (as expected) in the W+jets and $t\bar{t}$ samples, corresponding to W leptonic decays. However this is only a small fraction of the distribution and cutting on the transverse mass is again found not to improve the signal to background ratio over the minimal cuts.

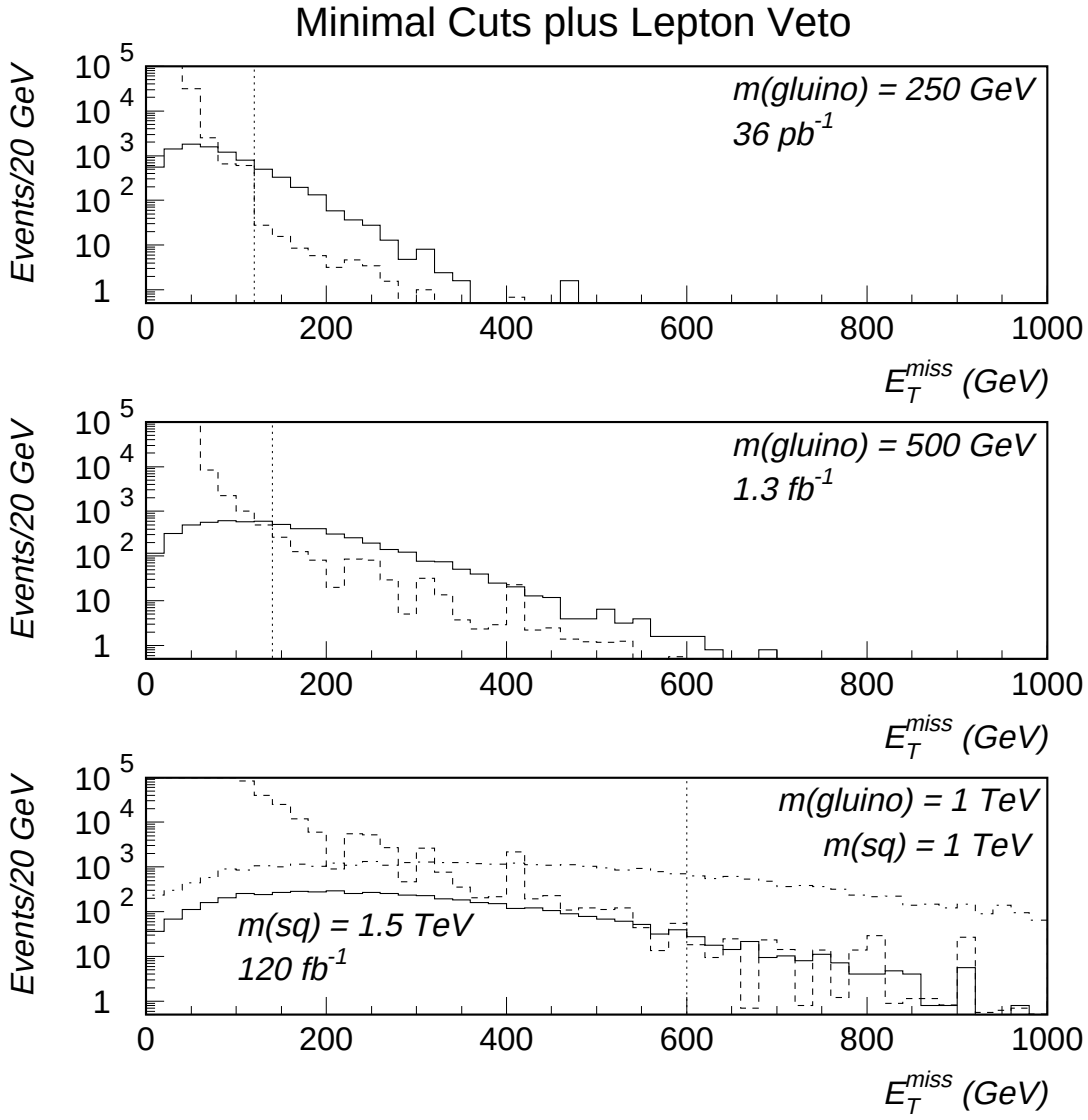

FIG. 13. Distributions of $\not\!\!E_T$ for supersymmetry signal events (solid) and the sum of all backgrounds (dashed), for SUSY I (upper row), SUSY II (middle row), and SUSY III and IV (lower row). Minimal cuts plus electron/muon veto were used. The signal statistics correspond to integrated luminosities of 36 pb^{-1}, 1.3 fb^{-1} and 120 fb^{-1} respectively; the background is normalized to the signal.

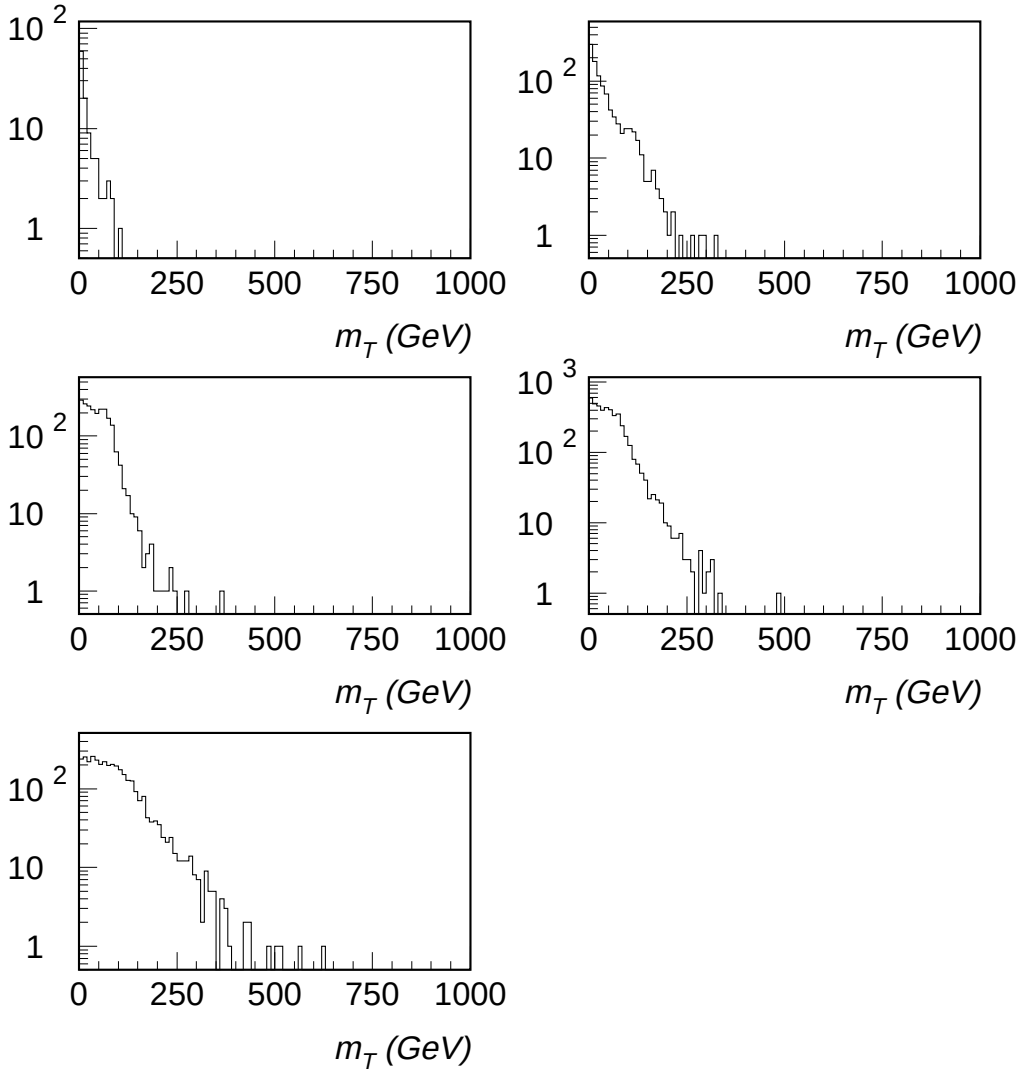

FIG. 14. Distributions of transverse mass for the leading electron/muon and $\not\!\!E_T$, for (a) QCD background, (b) Z+jets background, (c) W+jets background, (d) $t\bar{t}$ background, and (e) supersymmetry signal events (SUSY II).

WORST-CASE CALORIMETER RESOLUTION

The major detector effect is in the reducible background due to QCD jet mismeasurement. The question to be addressed is the effect of the calorimeter on the supersymmetry searches. In order to see how sensitive these searches are to the HCAL energy resolution, we have recomputed the QCD background using a "worst-case" resolution. (Only the QCD background was recomputed because, unlike the others, it has a significant component from calorimeter measurement rather than real $\not\!\!E_T$). The resolutions used were:

- $100\%/\sqrt{E} \oplus 5\%$ in the HCAL barrel;
- $150\%/\sqrt{E} \oplus 5\%$ in the HCAL endcap;
- $200\%/\sqrt{E} \oplus 10\%$ in the HV.

To simulate catastrophic energy mismeasurements, a non-Gaussian low-side tail with amplitude 0.2% and uniform distribution between zero and the incident energy was also included in the calorimeter response. The existing CMS HCAL testbeam dataset indicates that this is indeed a worst case.

The effect of this worsened resolution on the QCD background is shown in Fig. 15, which compares the distributions of $\not\!\!E_T$ for the baseline HCAL resolution, the worst-case resolutions, and the worst-case resolution without the non-Gaussian low side tail. As can be seen, the worst-case resolution significantly increases the contribution of the QCD background at moderate to large $\not\!\!E_T$ (by an order of magnitude for $\not\!\!E_T \sim 100-200$ GeV). The figure indicates that this effect is predominantly due to the non-Gaussian tail rather than the worsened Gaussian resolutions. Special care must therefore be taken to minimize such effects in the CMS calorimeter response.

The effect of the degraded resolution on the ability to observe a supersymmetry signal is shown in Fig. 16 (for the minimal cuts). Compared with Fig. 12 it will be seen that the background at low $\not\!\!E_T$ is enhanced significantly. The signal to background ratios in the signal region are slightly worse than in Fig. 12 but the supersymmetry signal can still be clearly seen. However, because the signal region is moved to higher $\not\!\!E_T$, the number of events per bin in the signal region is lower by a factor of about two compared with Fig. 12 indicating that with the worsened resolution one would have to run for about 1.4 times as long as the baseline case to obtain comparable significance.

EFFECT OF AN ECAL CRACK

We have also recomputed the QCD background under the assumption that the region of ECAL between $|\eta| = 1.5$ and 1.6 is dead, i.e. has zero response to the shower energy deposited in it by both hadrons and EM particles. This scenario is intended to model the possibility that cables and material in the region between barrel and endcap ECAL sections may contribute so much material as to absorb approximately the same fraction of shower energy as the ECAL would. The HCAL behind this region remains live and measures the expected fraction of shower energies.

The effect of this ECAL crack on the QCD background is shown in Fig. 17, which compares the distributions of $\not\!\!E_T$ for the baseline calorimeter and for the case with ECAL dead for $1.5 \leq |\eta| \leq 1.6$. As can be seen, the ECAL crack increases the contribution of the QCD background at large $\not\!\!E_T$ somewhat.

The effect of this degraded resolution on the ability to observe a supersymmetry signal is shown in Fig. 18 (for the minimal cuts). Compared with Figs. 12 and 16 it will be seen that the background at low $\not\!\!E_T$ is enhanced, but by less than in the case of the worst-case HCAL resolution. The signal to background ratios in the signal region are slightly worse than in Fig. 12 but the supersymmetry signal can still be clearly seen.

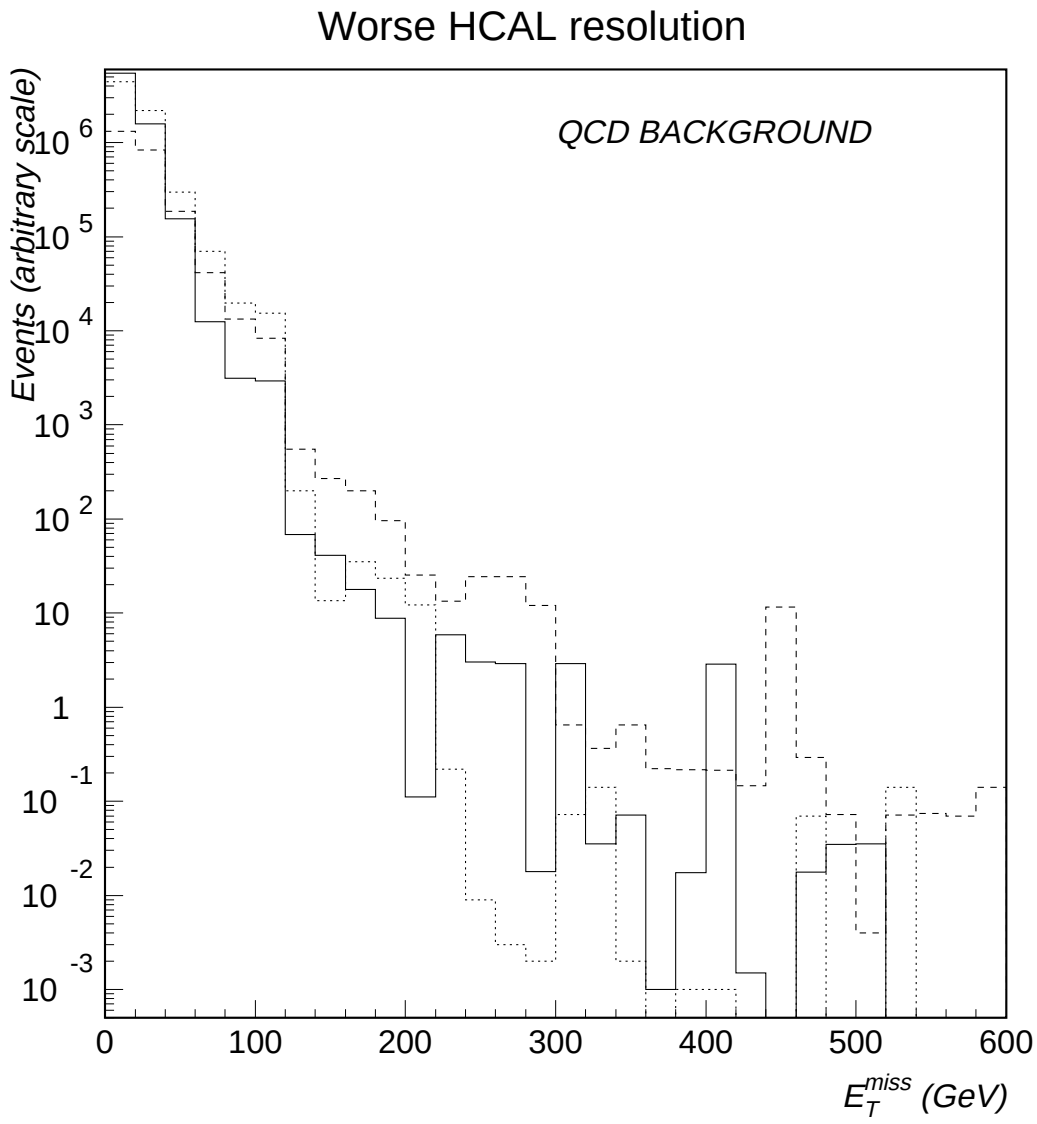

FIG. 15. Distributions of $\not\!\!E_T$ for QCD background events: baseline HCAL resolution (solid), worst-case resolutions (dashed), and worst-case resolution without the non-Gaussian low side tail (dotted).

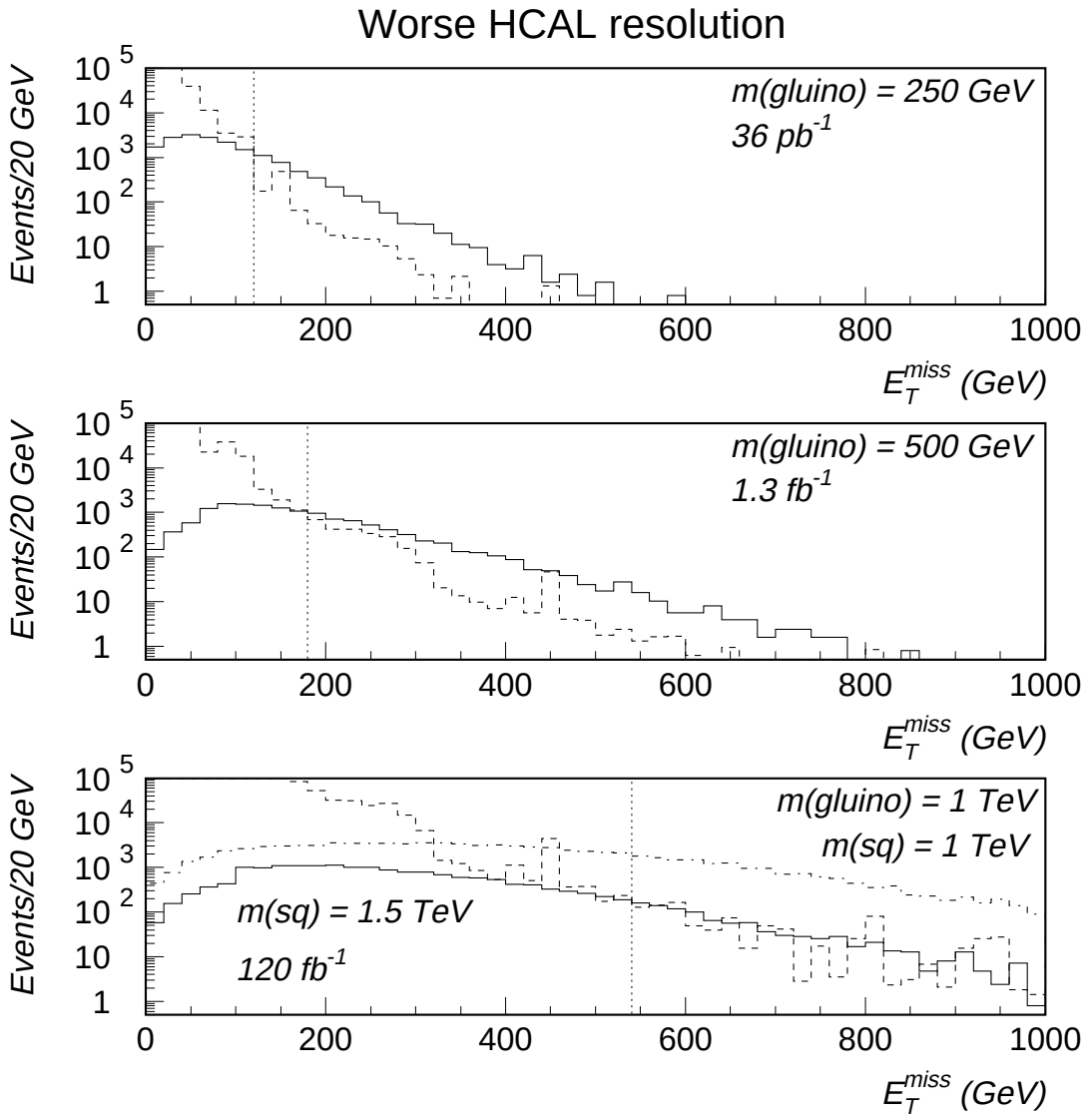

FIG. 16. Distributions of $\not\!\!E_T$ for supersymmetry signal events (solid) and the sum of all backgrounds (dashed), for SUSY I (upper row), SUSY II (middle row), and SUSY III and IV (lower row). Minimal cuts with "worst-case" HCAL resolutions were used. The signal statistics correspond to integrated luminosities of 36 pb^{-1}, 1.3 fb^{-1} and 120 fb^{-1} respectively; the background is normalized to the signal.

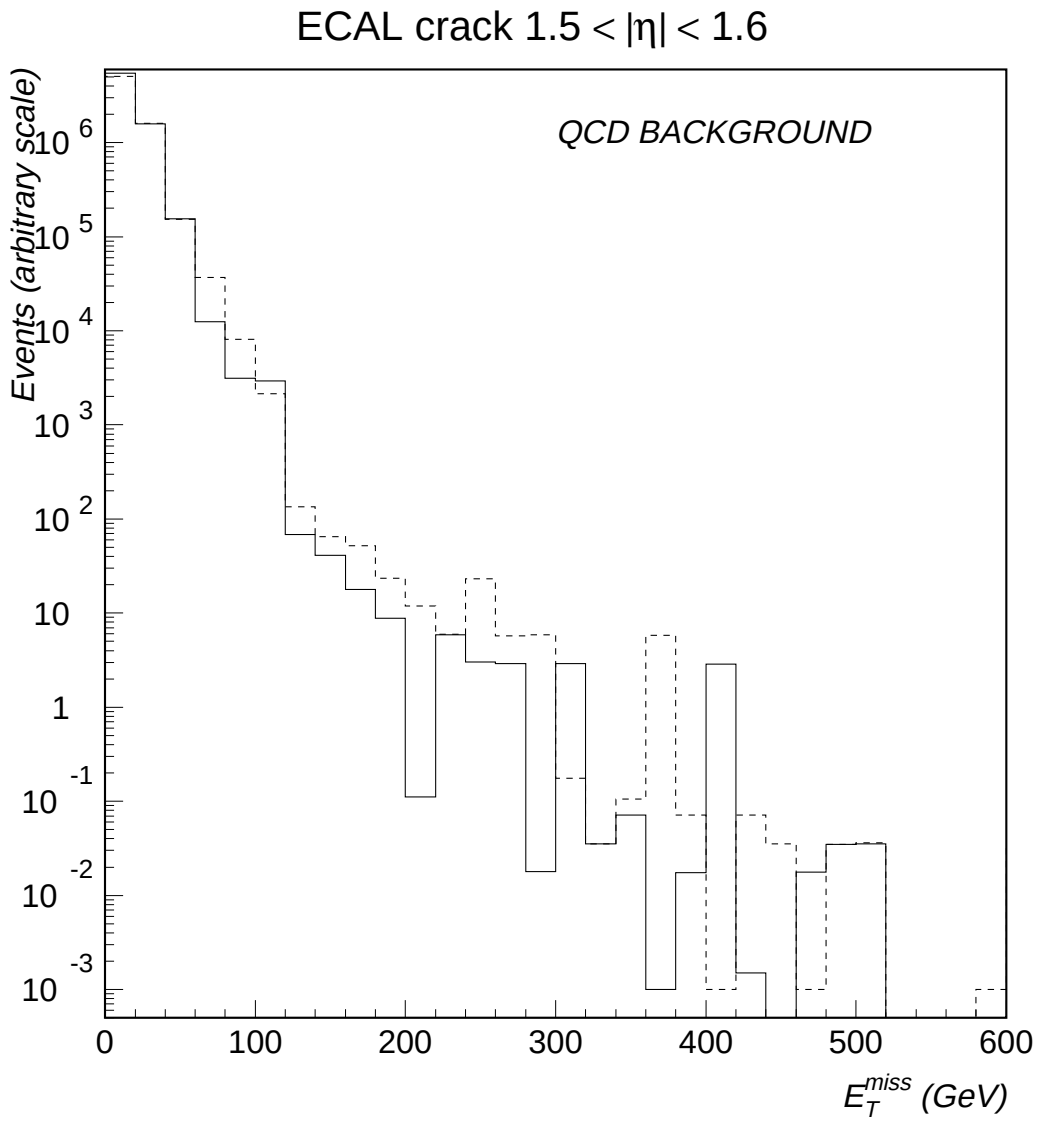

FIG. 17. Distributions of $\not\!\!E_T$ for QCD background events: baseline calorimeter (solid), and ECAL dead for $1.5 \leq |\eta| \leq 1.6$ (dashed).

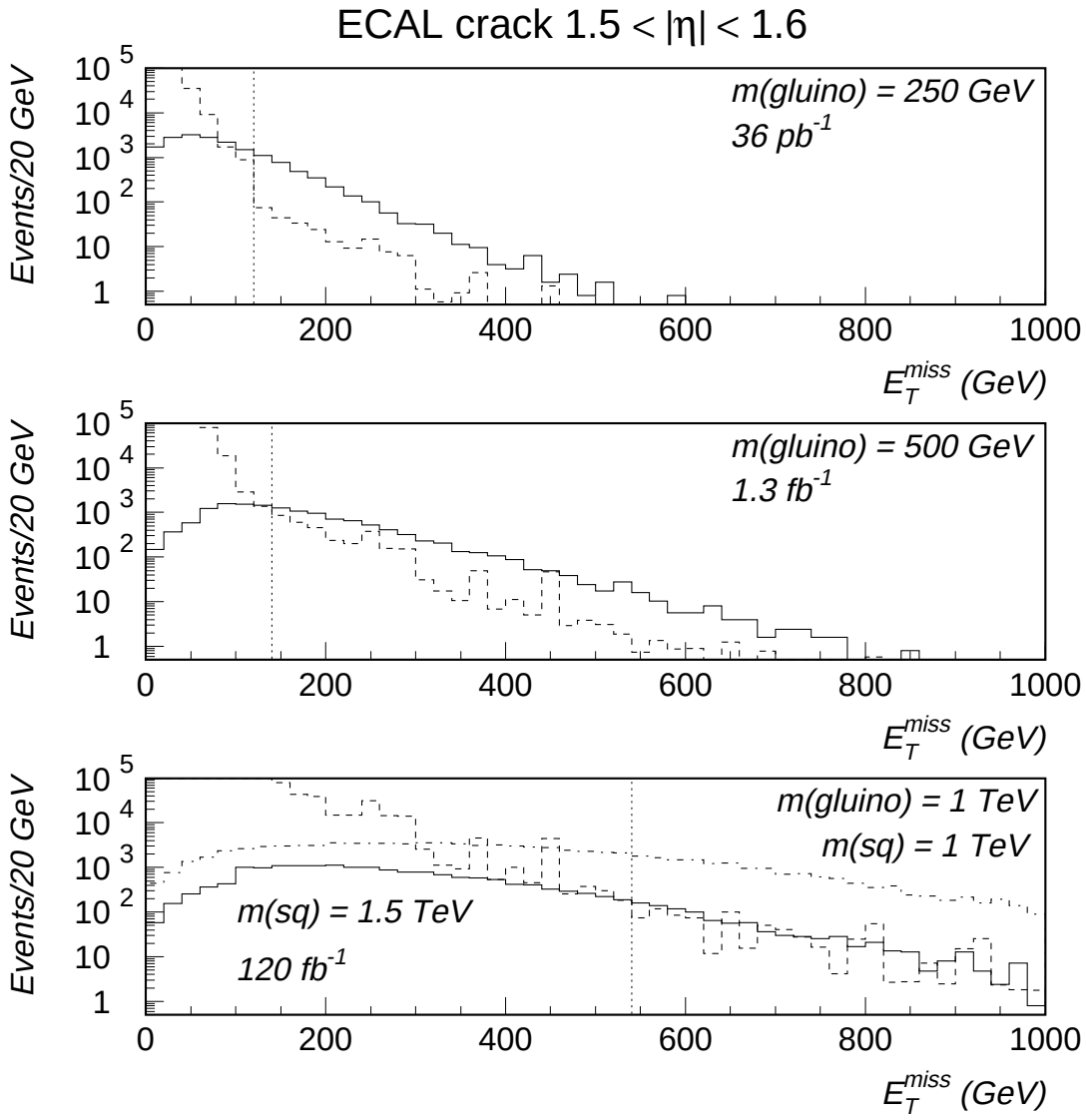

FIG. 18. Distributions of $\not\!\!E_T$ for supersymmetry signal events (solid) and the sum of all backgrounds (dashed), for SUSY I (upper row), SUSY II (middle row), and SUSY III and IV (lower row). Minimal cuts with ECAL dead for $1.5 \leq |\eta| \leq 1.6$ were used. The signal statistics correspond to integrated luminosities of 36 pb^{-1}, 1.3 fb^{-1} and 120 fb^{-1} respectively; the background is normalized to the signal.

EFFECT OF AN HCAL-VFCAL CRACK

We have also recomputed the QCD background under the assumption that the region between $|\eta| = 3.0$ and 3.1 is completely dead. This scenario is intended to model the a possible crack region between the endcap HCAL (HF) and the VFCAL (HV) calorimeter.

The effect of this HCAL-VFCAL crack on the QCD background is shown in Fig. 19, which compares the distributions of $\not\!\!E_T$ for the baseline calorimeter and for the case with the region $3.0 \leq |\eta| \leq 3.1$ dead. As can be seen, the dead region increases the contribution of the QCD background at large $\not\!\!E_T$ somewhat.

The effect of this degraded resolution on the ability to observe a supersymmetry signal is shown in Fig. 20 (for the minimal cuts). Compared with Figs. 12, 16, and 18, it will be seen that the background at low $\not\!\!E_T$ is enhanced, but the effect is rather less than in the case of the ECAL crack. The signal to background ratios in the signal region are only marginally worse than in Fig. 12 and the supersymmetry signal can still be clearly seen.

COMBINED EFFECT

If all these effects (worse HCAL resolution, ECAL crack and HCAL-VFCAL crack) are combined, the effect on the QCD background is shown in Fig. 21. As can be seen, the dead region increases the contribution of the QCD background at moderate to large $\not\!\!E_T$ significantly.

The effect of this degraded resolution on the ability to observe a supersymmetry signal is shown in Fig. 22 (for the minimal cuts). Compared with Fig. 12, it will be seen that the background at low $\not\!\!E_T$ is enhanced, and thus the signal region is shifted to higher $\not\!\!E_T$. While the supersymmetry signal can still be clearly seen, the number of events per bin in the signal region is a factor 2.5 times lower than the baseline case for SUSY I, so one would have to run for 1.6 times longer to obtain a comparable significance. (The effect on the higher masses is less severe but not negligible).

EFFECT OF MATERIAL BETWEEN ECAL AND HCAL

We have also recomputed the QCD background using a degraded HCAL response function designed to model the effect of 0.6 absorption lengths of dead material between the rear of the ECAL crystals and the front face of HCAL. Energy is lost in this dead material and this has the effect of introducing a low-side tail to the hadronic response. The effect was quantified using hanging file testbeam data by excluding certain readout layers, and parametrized as: [5]

$$P(E_{loss}/E) \propto e^{-E_{loss}/0.067E}.$$

The effect of this response function on the QCD background is shown in Fig. 23, which compares the distributions of $\not\!\!E_T$ for the baseline calorimeter and for the case with energy losses in ECAL-HCAL dead material. As can be seen, the dead material increases the contribution of the QCD background at moderate $\not\!\!E_T$ significantly (by two orders of magnitude for $\not\!\!E_T \sim 150$ GeV.

The effect of this degraded resolution on the ability to observe a supersymmetry signal is shown in Fig. 24 (for the minimal cuts). Compared with Fig. 12, the background at low $\not\!\!E_T$ is enhanced, and again the signal region is shifted to higher $\not\!\!E_T$. While the supersymmetry signal can still be clearly seen, the number of events per bin in the signal region is a factor 4 times lower than the baseline case for SUSY I, so one would have to run for twice as long to obtain a comparable significance. (The effect on the higher mass SUSY signals is less severe since this choice of response function does not create a large enhancement at large $\not\!\!E_T$.)

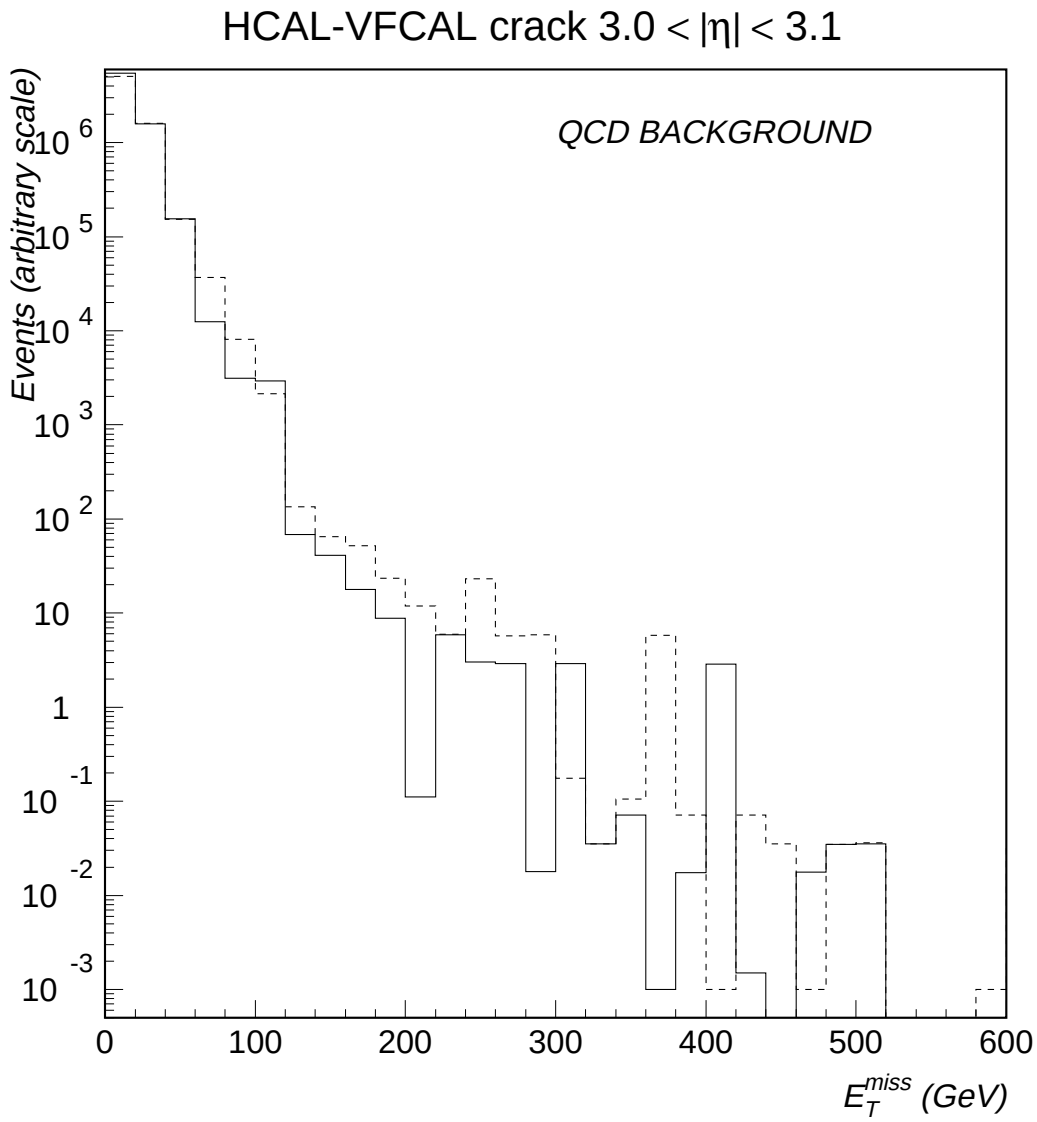

FIG. 19. Distributions of $\not\!\!E_T$ for QCD background events: baseline calorimeter (solid), and HCAL-VFCAL crack $3.0 \leq |\eta| \leq 3.1$ (dashed).

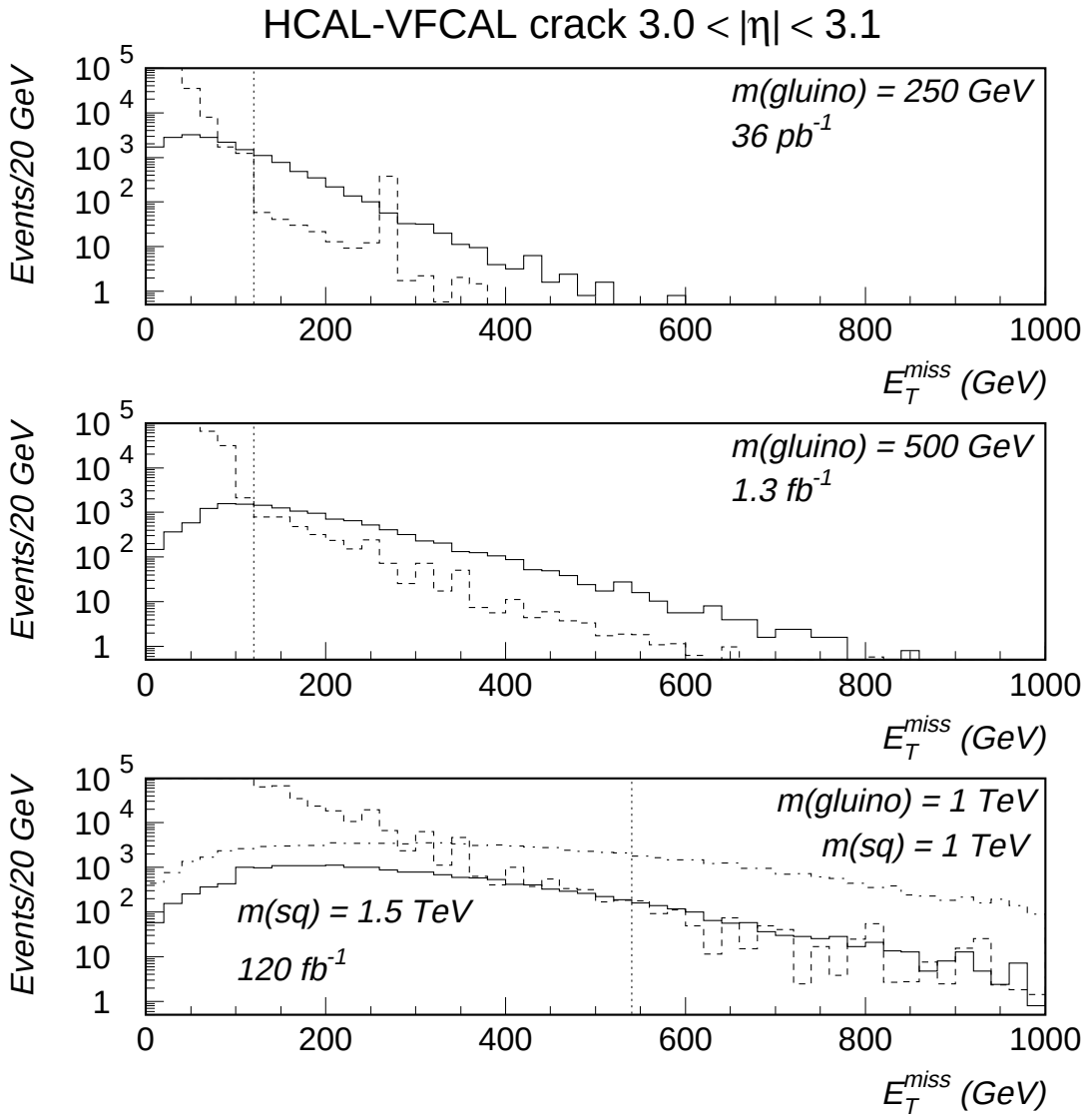

FIG. 20. Distributions of $\not\!\!E_T$ for supersymmetry signal events (solid) and the sum of all backgrounds (dashed), for SUSY I (upper row), SUSY II (middle row), and SUSY III and IV (lower row). Minimal cuts with dead region for $3.0 \leq |\eta| \leq 3.1$ were used. The signal statistics correspond to integrated luminosities of 36 pb^{-1}, 1.3 fb^{-1} and 120 fb^{-1} respectively; the background is normalized to the signal.

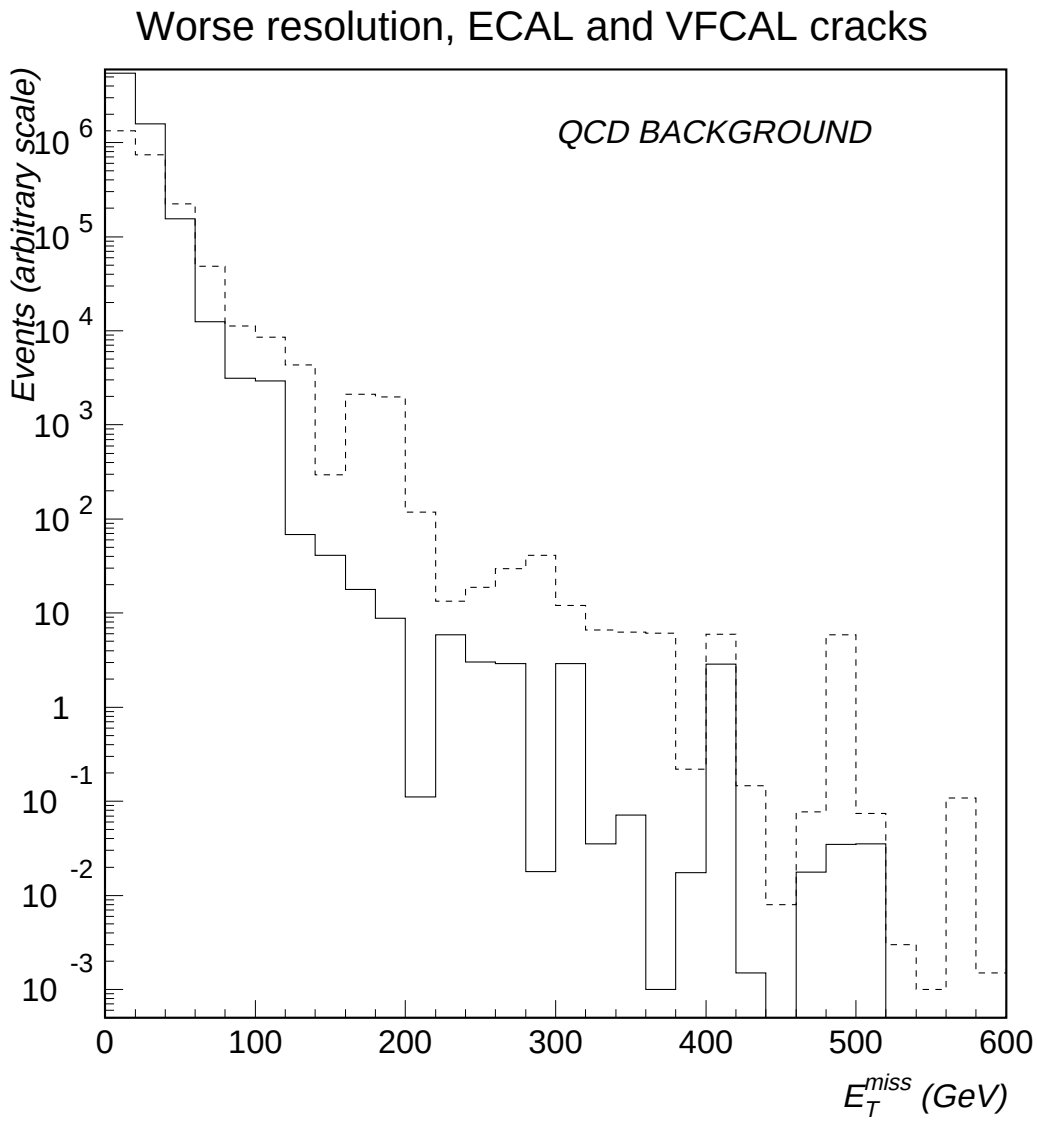

FIG. 21. Distributions of $\not\!\!E_T$ for QCD background events: baseline calorimeter (solid), and HCAL-VFCAL crack $3.0 \leq |\eta| \leq 3.1$ (dashed).

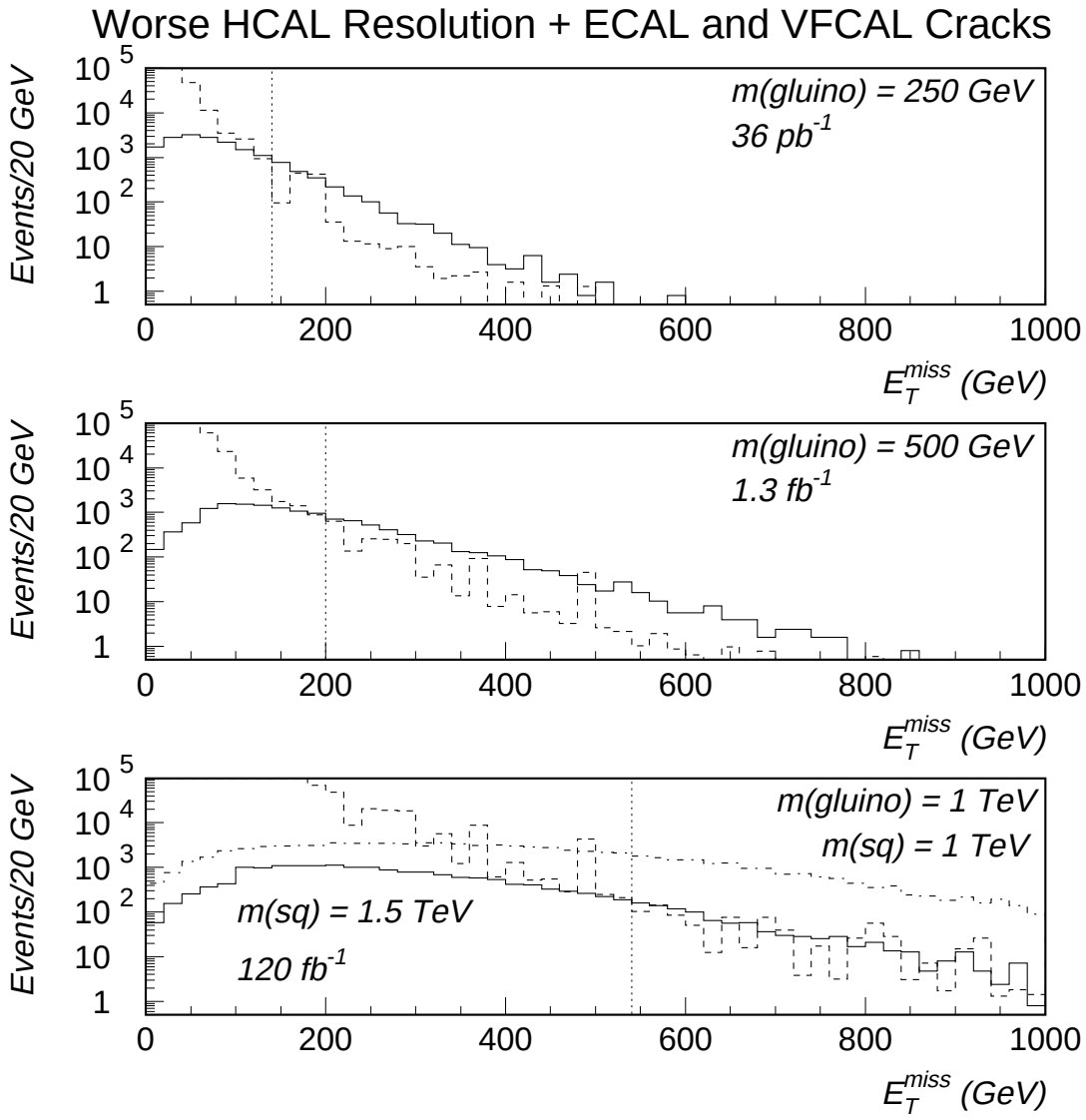

FIG. 22. Distributions of $\not\!\!E_T$ for supersymmetry signal events (solid) and the sum of all backgrounds (dashed), for SUSY I (upper row), SUSY II (middle row), and SUSY III and IV (lower row). Minimal cuts with dead region for $3.0 \leq |\eta| \leq 3.1$ were used. The signal statistics correspond to integrated luminosities of 36 pb^{-1}, 1.3 fb^{-1} and 120 fb^{-1} respectively; the background is normalized to the signal.

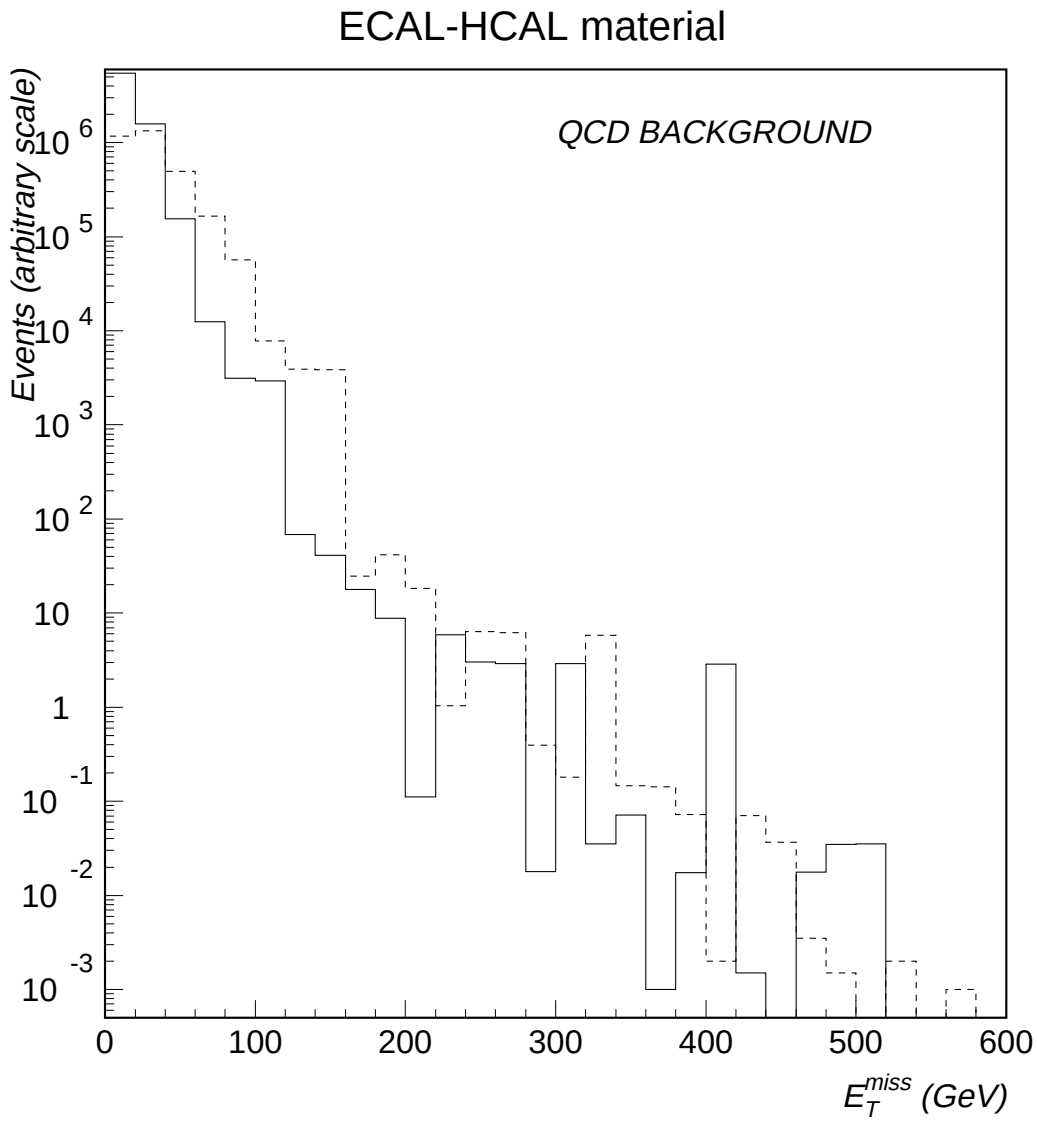

FIG. 23. Distributions of $\not\!\!E_T$ for QCD background events: baseline calorimeter (solid), and response function with ECAL-HCAL dead material (dashed).

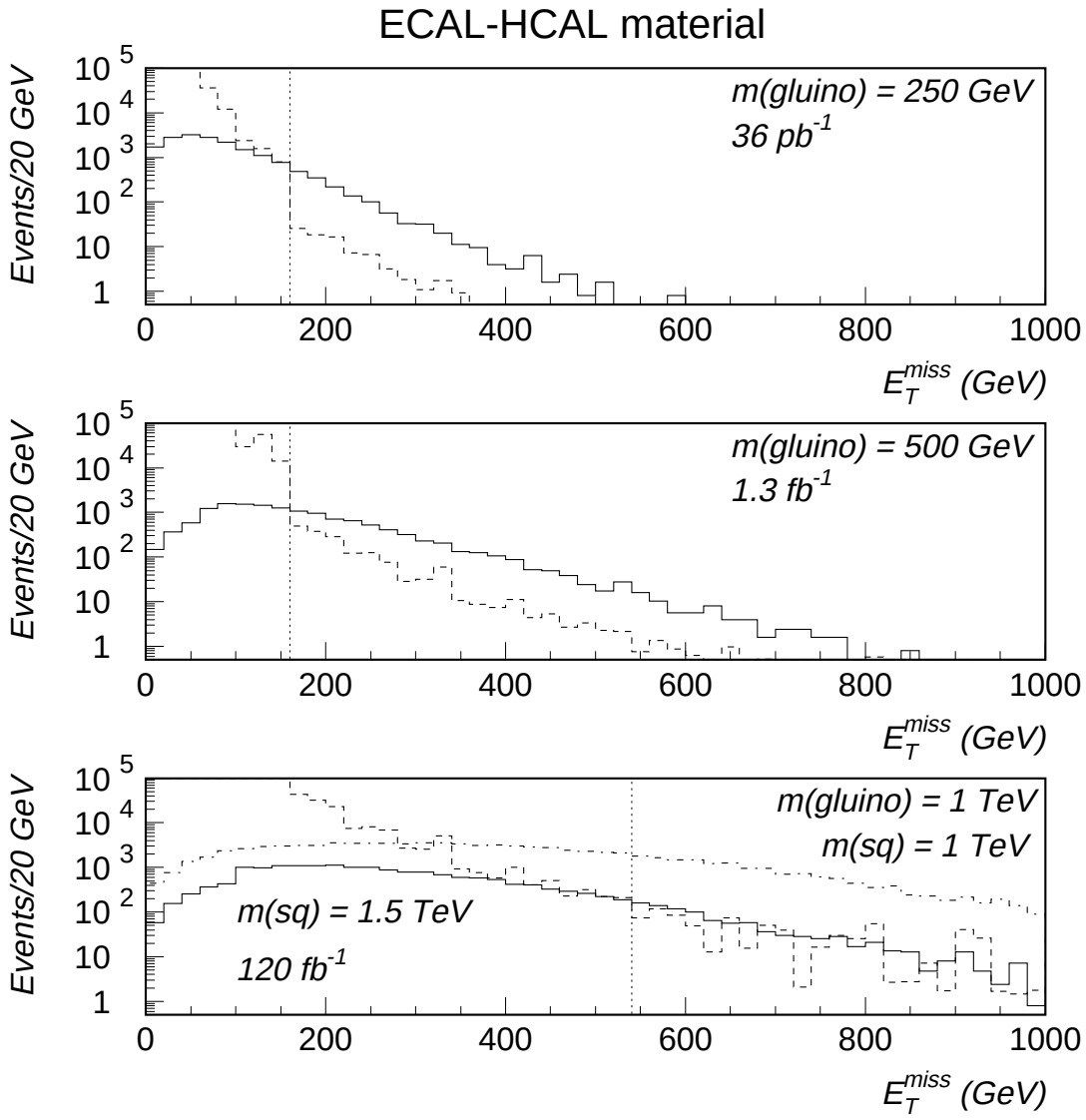

FIG. 24. Distributions of $\not\!\!E_T$ for supersymmetry signal events (solid) and the sum of all backgrounds (dashed), for SUSY I (upper row), SUSY II (middle row), and SUSY III and IV (lower row). Minimal cuts with dead material between ECAL and HCAL were used. The signal statistics correspond to integrated luminosities of 36 pb^{-1}, 1.3 fb^{-1} and 120 fb^{-1} respectively; the background is normalized to the signal.

SUMMARY AND CONCLUSIONS

- CMS can detect a supersymmetry signal above backgrounds in the $\not\!\!E_T$+jets channel up to $m_{\tilde{g}} \sim 1\,\mathrm{TeV}$ with an integrated luminosity of 100 fb^{-1}. This covers the entire range over which supersymmetry models relevant to electroweak symmetry breaking make sense [4].
- Worst-case HCAL resolutions increase the QCD background significantly at low $\not\!\!E_T$ and would increase the luminosity required to observe a supersymmetry signal with a given significance by a factor of about 1.4.
- Non-Gaussian contributions to the calorimeter response have an especially bad effect on $\not\!\!E_T$, so care must be taken to avoid such effects.
- A dead region of size $\Delta\eta = 0.1$ in the ECAL (as might be caused by cables between barrel and endcap ECAL sections) also increases the QCD background and again would increase the luminosity required for observation of a supersymmetry signal with a given significance.
- A dead region of size $\Delta\eta = 0.1$ between the HCAL (HF) and VFCAL (HV) has less of an effect than this.
- Dead material between ECAL and HCAL leads to a low-side tail in the hadronic energy response which also increases the QCD background. This significantly increases the luminosity required to observe a low-mass SUSY signal.

A somewhat subjective ranking of the seriousness of the effects studied would be:

1. Non-Gaussian response due to ECAL-HCAL material and/or tails, is worse than:
2. Cracks of size $|\Delta\eta| = 0.1$, which are worse than:
3. Degraded but still Gaussian calorimeter resolution.

The need to maintain good missing E_T resolution must continue to be considered at all stages of the design and integration process for the CMS detector, since apparently small design compromises can have major impacts on our ability to observe missing E_T signals.

REFERENCES

1. 'Report of the TeV2000 Study Group on Future Electroweak Physics at the Tevatron,' D. Amidei and R. Brock (eds.), Fermilab 1996.
2. A. Beretvas *et al.*, 'SSCSIM: Development and Use by the Fermilab SDC Group,' in Proc. of MC93, The International Conference on Monte Carlo Simulations in High Energy and Nuclear Physics, Tallahassee, Florida, February 1993.
3. A. Beretvas *et al.*, CMS–TN/94-326.
4. R. Arnowitt, private communication.
5. D. Green, private communication.